eNeuro Accepted Manuscript

eNeuro

Research Article: New Research | Disorders of the Nervous System

Amyloid Precursor Protein (APP) controls the expression of the transcriptional activator Neuronal PAS Domain Protein 4 (NPAS4) and synaptic GABA release

https://doi.org/10.1523/ENEURO.0322-19.2020

Cite as: eNeuro 2020; 10.1523/ENEURO.0322-19.2020

Received: 14 August 2019
Revised: 13 March 2020
Accepted: 17 March 2020

This Early Release article has been peer-reviewed and accepted, but has not been through the composition and copyediting processes. The final version may differ slightly in style or formatting and will contain links to any extended data.

Alerts: Sign up at www.eneuro.org/alerts to receive customized email alerts when the fully formatted version of this article is published.

Copyright © 2020 Opsomer et al.
This is an open-access article distributed under the terms of the Creative Commons Attribution 4.0 International license, which permits unrestricted use, distribution and reproduction in any medium provided that the original work is properly attributed.

eNeuro Accepted Manuscript

1. Manuscript Title (50 word maximum)

Amyloid Precursor Protein (APP) controls the expression of the transcriptional activator Neuronal PAS Domain Protein 4 (NPAS4) and synaptic GABA release

2. Abbreviated Title (50 character maximum)

APP-dependent GABA release

3. Author Names and Affiliations

Rémi Opsomer[1], Sabrina Contino[1†], Florian Perrin[1,2†], Roberta Gualdani[4], Bernadette Tasiaux[1], Pierre Doyen[3], Maxime Vergouts[3], Céline Vrancx[1], Anna Doshina[1], Nathalie Pierrot[1], Jean-Noël Octave[1], Philippe Gailly[4], Serena Stanga[1#], Pascal Kienlen-Campard[1*].

[1] CEMO-Alzheimer Dementia group, Institute of Neuroscience, Université catholique de Louvain, Brussels, Belgium.

[2] de Duve Institute, Ludwig Institute for Cancer Research and Université catholique de Louvain, Brussels, Belgium.

[3] CEMO-Laboratory of Neuropharmacology, Institute of Neuroscience, Université catholique de Louvain, Brussels, Belgium.

[4] CEMO-Laboratory of Cell Physiology, Institute of Neuroscience, Université catholique de Louvain, Brussels, Belgium.

[#] *Current address*: Neuroscience Institute Cavalieri Ottolenghi, Department of Neuroscience, University of Torino, Torino, Italy

[†]These authors have contributed equally to this work.

4. Author Contributions:

RO Performed Research and Wrote the paper. SC, FP, PG and RG Performed Research and Analyzed data. BT, PD, MV, CV and AD Performed Research. NP and JNO Analyzed data. SS Analyzed data and wrote the paper. PKC Designed Research and wrote the paper.

5. Correspondence should be addressed to:

Pascal Kienlen-Campard
Institute of Neuroscience
IONS-CEMO, Avenue Mounier 53 bte B1.53.02
B-1200 Brussels
Belgium
Phone: +32 2 764 93 35
Fax : +32 2 764 54 60
Email: pascal.kienlen-campard@uclouvain.be

eNeuro Accepted Manuscript

6. Number of Figures

14 (7 Figures, 7 Extended Data Figures)

7. Number of Tables

/

8. Number of Multimedia

/

9. Number of words for Abstract

247

10. Number of words for Significance Statement

118

11. Number of words for Introduction

739

12. Number of words for Discussion

1648

13. Acknowledgements

pLenti CMV/TO Puro empty (w175-1) was a gift from Eric Campeau & Paul Kaufman (Addgene plasmid #17482). pL-CRISPR.EFS.GFP (Addgene plasmid # 57818) and pL-CRISPR.EFS.tRFP (Addgene plasmid # 57819) were a gift from Benjamin Ebert. pCMV delta R8.2 (Addgene plasmid # 12263) and pMD2.G (Addgene plasmid # 12259) were a gift from Didier Trono. We thank Jerome Ambroise for insight and technical support in the analysis of microarray data, and Xavier Yerna for technical support in electrophysiology. We thank Nicolas Dauguet for the cell cytometry sorting of the neurons. We thank Devkee Mahesh Vadukul for her critical and linguistic revision of the manuscript.

14. Conflict of Interest:

Authors report no conflict of interest

15. Funding sources

This work was supported by the Belgian Fonds pour la formation à la recherche dans l'industrie et l'agriculture (FRIA-FNRS), the Interuniversity Attraction Pole Programme-Belgian Sate-Belgian Science Policy (IAP-P7/16 and IAP-P7/13), The Belgian Fonds de la Recherche Scientifique Médicale (FRSM), the Queen Elisabeth Medical Foundation (FMRE), the Fondation

eNeuro Accepted Manuscript

pour la Recherche sur la Maladie d'Alzheimer (SAO/FRA) and by the Concerted Research Action from the General Direction of Scientific Research of the French Community of Belgium, (ARC 14/19-059 and ARC17/22-083).

eNeuro Accepted Manuscript

Abstract

The Amyloid Precursor Protein (APP) has been extensively studied as the precursor of the β-amyloid peptide (Aβ) peptide, the major component of the senile plaques found in the brain of Alzheimer's disease (AD) patients. However, the function of APP *per se* in neuronal physiology remains to be fully elucidated. APP is expressed at high levels in the brain. It resembles a cell adhesion molecule or a membrane receptor, suggesting that its function relies on cell-cell interaction and/or activation of intracellular signaling pathways. In this respect, the APP intracellular domain (AICD) was reported to act as a transcriptional regulator. Here, we used a transcriptome-based approach to identify the genes transcriptionally regulated by APP in the rodent embryonic cortex and upon maturation of primary cortical neurons. Surprisingly, the overall transcriptional changes were subtle, but a more detailed analysis pointed to genes clustered in neuronal-activity dependent pathways. In particular, we observed a decreased transcription of Neuronal PAS domain protein 4 (NPAS4) in APP-/- neurons. NPAS4 is an inducible transcription factor (ITF) regulated by neuronal depolarization. The down-regulation of NPAS4 co-occurs with an increased production of the inhibitory neurotransmitter GABA and a reduced expression of the $GABA_A$ receptors alpha1. CRISPR-Cas-mediated silencing of NPAS4 in neurons led to similar observations. Patch-clamp investigation did not reveal any functional decrease of $GABA_A$ receptors activity, but LTP measurement supported an increased GABA component in synaptic transmission of APP-/- mice. Together, NPAS4 appears to be a downstream target involved in APP-dependent regulation of inhibitory synaptic transmission.

eNeuro Accepted Manuscript

106 **Significance Statement**

107 The Amyloid Precursor Protein (APP) is a key player in Alzheimer's disease (AD) pathogenesis.
108 We report the down-regulation of the activity-dependent transcription factor Neuronal PAS
109 domain protein 4 (NPAS4) in APP-deficient neurons, along with an increase in GABAergic
110 neuron markers and GABA release, but not in excitatory glutamatergic markers. We identified
111 NPAS4 as an APP target gene by a transcriptome analysis of APP+/+ versus APP-/- primary
112 cortical neurons at different stages of differentiation. The downregulation of NPAS4 observed in
113 APP-/- neurons was confirmed by APP silencing with a CRISPR/Cas9 approach. CRISPR/Cas9-
114 silencing of NPAS4 mimicked APP deficiency and increased GABAergic markers. The activity-
115 dependent transcription factor NPAS4 is therefore a key downstream target in the synaptic
116 functions regulated by APP.

117

eNeuro Accepted Manuscript

Introduction

The physiological functions of APP *per se* have been largely overlooked in comparison with its role of precursor of the Aβ peptide. Aβ deposition is a central event in AD, but alterations of APP physiological functions are likely to play a key role in the pathogenesis.

APP belongs to the APP-like protein family (with APLP1 and APLP2, referred to as APLPs), expressed in most of the species. The APLP family results from several duplications and contraction events during evolution. The specific functions ascribed to each member are yet not clearly defined (for a review see Shariati and De Strooper, 2013). APP-/- mice show a subtle phenotype, with reduced body and brain weight, reduced locomotor activity, gliosis, mild axonal growth/white matter defects (Guo et al., 2012; Muller et al., 2012; Muller and Zheng, 2012). However, a large range of functions have been attributed to APP including neuronal proliferation, differentiation (Freude et al., 2011; Hu et al., 2013) and migration during embryogenesis (Young-Pearse et al., 2007). APP promotes neurite outgrowth (Hoe et al., 2009b), synapse formation and activity (Priller et al., 2006; Santos et al., 2009; Lee et al., 2010; Pierrot et al., 2013; Klevanski et al., 2015; Zou et al., 2016) in the central nervous system (CNS) or at the neuromuscular junction (Stanga et al., 2016). APP modulates the excitatory neurotransmission by interacting with AMPA (Lee et al., 2010) or NMDA receptors (Cousins et al., 2009; Hoe et al., 2009a). APP deficiency reduces paired pulse depression (PPD) in mice (Seabrook et al., 1999) and affects the expression of GABA receptors (Fitzjohn et al., 2000; Chen et al., 2017). Its overexpression induces hyperexcitability due to failure in GABAergic neurotransmission (Born et al., 2014), and triggers the GABA excitatory/inhibitory shift occurring during neuronal maturation (Doshina et al., 2017).

Tuning inhibitory/excitatory neurotransmission is instrumental in neuronal plasticity and memory formation. This process is regulated by a set of transcription factors known as inducible transcription factors or ITFs. ITFs belong to the Immediate Early Genes (IEGs) family, and are

eNeuro Accepted Manuscript

143 sensitive to neuronal activity. They control the mechanisms that “reshape” synaptic inputs on
144 neurons (West and Greenberg, 2011), and play a key role in neuronal plasticity and memory
145 formation (Alberini, 2009; Loebrich and Nedivi, 2009; Leslie and Nedivi, 2011). Among them,
146 NPAS4 is robustly expressed upon neuronal depolarization, and is involved in a transcriptional
147 program that regulates neuronal firing responses to excitatory transmission by enhancing
148 inhibition (Lin et al., 2008). Elevated activity of inhibitory neurons also induces NPAS4,
149 promoting increased excitation onto the same neurons (Spiegel et al., 2014).

150 The molecular mechanisms underlying APP functions are still elusive, but several studies
151 reported that APP function is mediated by the transcriptional regulation of so-called APP target
152 genes, which is operated by the APP intracellular domain (AICD). An increasing list of AICD
153 candidate genes has emerged from various models (reviewed in Pardossi-Piquard and Checler,
154 2012). On the other hand, APP was also reported to regulate gene transcription independently of
155 AICD release (Hicks et al., 2013; Pierrot et al., 2013). It is thus so far quite impossible to clearly
156 define (i) the precise identity of APP target genes in neurons (ii) the related molecular pathways
157 underlying APP-dependent gene transcription (iii) how APP target genes relate to APP neuronal
158 function.

159 In this study, we first aimed at identifying genes that are transcriptionally regulated by APP in
160 primary neurons. We performed a transcriptome analysis (APP+/+ vs. APP-/-) in primary cortical
161 neurons at different stages of differentiation. Changes observed in global gene expression in the
162 absence of APP were subtle. A more detailed pathway analysis indicated that expression of
163 genes clustered in activity-dependent pathway, and among these the ITF NPAS4, were down-
164 regulated in the absence of APP after 7 days of culture. Strikingly, we observed that the amount
165 of the inhibitory neurotransmitter GABA (γ-aminobutyric acid) was increased in APP-/- neurons.
166 This was supported by an increased expression of the Glutamate Decarboxylase 65 (GAD65) in
167 the same context. Glutamate levels were not altered in APP-/- neurons. These observations

eNeuro Accepted Manuscript

were reproduced upon acute silencing of APP by CRISPR-Cas9 editing. The knockdown of NPAS4 gave similar results. Neurophysiological investigations showed that excitatory postsynaptic potentials (EPSP) consecutive to a Theta-burst stimulation (TBS) decreased in APP-/- supporting the increase release GABA, and suggesting increased inhibitory synaptic inputs in APP-/- neurons. Altogether, our data provide new insight into APP-dependent neuronal activity, indicating that NPAS4 is an APP downstream target gene, tuning the GABA-dependent activity in neuronal networks.

eNeuro Accepted Manuscript

Materials and Methods

Antibodies, chemicals and reagents

All media and reagents used for cell cultures were purchased from Thermo Fisher Scientific (Waltham, USA); Fetal Bovine Serum (FBS) was purchased from Biowest (Nuaillé, France). Analytical grade solvents and salts were purchased from Sigma-Aldrich (St-Louis, USA). sAPPα (S9564) and DAPI (D9542) were from Sigma-Aldrich (St-Louis, USA), Triton-X100 from Merck (Darmstadt, Germany) and TriPure Isolation Reagent from Roche (Basel, Switzerland). Microarray analysis kits were from Affymetrix (Santa Clara, USA). All reagents for RNA processing or cDNA synthesis were from Bio-Rad (Hercules, USA), and primers were from Sigma-Aldrich (St Louis, USA). BCA Protein Assay kit was from Thermo Fisher Scientific (Waltham, USA). NuPAGE® reagents were from Invitrogen (Carlsbad, USA). PolyVinyliDene Fluoride (PVDF) and nitrocellulose membranes were from Merck Millipore (Billerica, USA) or Amersham™ (Little Chalfont, UK). Nonfat dry milk was from Merck (Darmstadt, Germany). Western Lighting® Plus-ECL reagents were from PerkinElmer (Waltham, USA) and Fluoprep mounting medium from bioMérieux (Marcy l'Etoile, France). Lentivirus were prepared with Acrodisc® 0,45µm filters (Pall, NYC, USA) and LentiX™ Concentrator reagent (Clontech, Mountain View, USA).

The following antibodies were used: APP NT 22C11 (Cat. No. MAB348, Merck Millipore, Billerica, USA), anti-human APP W0-2 (Cat. No.MABN10, Merck Millipore, Billerica, USA), anti-APP CT Y188 (Cat. No. ab32136 Abcam, Cambridge, UK), anti-APLP1 (Cat. No. 171615, Calbiochem EMD Biosciences – Merck, Darmstadt, Germany), anti-APLP2 (Cat. No. 171616, Calbiochem EMD Biosciences – Merck, Darmstadt, Germany), anti-GAPDH 14C10 (Cat. No. 2118, Cell Signaling, Danvers, USA), anti-MAP2 (Cat. No. M4403, Sigma-Aldrich St Louis, USA), anti-GAD65 (D5G2, Cat. No. 5843 Cell Signaling, Danvers, USA), anti-mouse IgG, HRP Whole antibody anti-rabbit IgG HRP (Cat. No. NA931-1ML, Amersham, Little Chalfont, UK),

eNeuro Accepted Manuscript

whole goat anti-mouse antibody (Cat. No. NA934-1ML, Amersham, Little Chalfont, UK) Alexa Fluor®-488, goat anti-mouse; Alexa Fluor®-568, goat anti-rabbit; Alexa Fluor®-647 and DAPI were purchased from ThermoFisher Scientific (Waltham, USA). Glutamate assay kit was from Abcam (Cambridge, UK) and γ-aminobutyric acid (GABA) ELISA from Cloud-Clone Corporation. 70 µm Falcon™ Cell Stainers were from ThermoFisher Scientific (Waltham, USA).

Animal models

All animal procedures were performed in accordance with the regulations and policies of the University animal care committee. APP+/+ and APP-/- mice were obtained from the Jackson Laboratory (Bar Harbor, USA) as C57Bl6/J and backcrossed for > 6 generations in CD1 genetic background. Animals were housed on a 12 h light/dark cycle in standard animal care facility with access to food and water *ad libitum*. Heterozygous animals (APP+/-) were bred and crossed to obtain embryos of either sex from the three different genotypes (APP+/+, APP+/- and APP-/-) in the same litter.

Primary culture and treatments

Primary cultures of cortical neurons were prepared from E18 mouse embryos. Cortices were dissected and dissociated in HBSS without calcium and magnesium and the mixture was centrifuged on FBS for 10 min at 1,000 x g to pellet cells. Cells were plated at 200,000 cells/cm² in culture dishes pre-treated with 10 µg/ml of poly-L-lysine in phosphate buffered saline (PBS) and cultured (37°C, 5% CO_2 and humidified atmosphere). Cells were cultured for 3 to 14 days *in vitro* in Neurobasal® medium enriched with 2% v/v B-27® supplement medium and 1 mM L-glutamine. Half of the medium was renewed every 2-3 days. Treatments with 20 nM of soluble APPα (sAPPα) were performed for 16 h after 6 days of culture (DIV6).

For primary cultures of astrocytes, cortices from pups were collected at postnatal day 2 and mechanically dissociated. Astrocytes were isolated using a 30% Percoll gradient and seeded

eNeuro Accepted Manuscript

into gelatin-coated tissue culture flasks. Cells were left to proliferate for 14 days at 37°C - 5% CO_2 in DMEM-glutaMAX medium supplemented with 10% FBS, 50 mg/ml penicillin–streptomycin and 50 mg/ml fungizone. Medium was renewed after 7 days, cells were passaged after 14 days and further cultured in DMEM-glutaMAX with 10% FBS. Two days after passage, FBS was reduced to 3% and medium was supplemented with the growth factor cocktail G5. All experiments/treatments were performed 7 days after, referred to as DIV7 for astrocytes. For NPAS4-induction analysis, neurons and astrocytes at DIV7 were depolarized with 50 mM KCl for 2-4h.

RNA extraction, transcriptome analysis and qRT-PCR

Total RNA was extracted by TriPure Isolation Reagent according to the manufacturer's protocol. RNA samples were suspended in DEPC-treated water and RNA concentration was measured (OD 260 nm) on BioSpec-nano spectrophotometer (Shimadzu Biotech). For microarray analysis, RNA quality was monitored by capillary electrophoresis using the Agilent 2100 Bioanalyzer instrument with the Agilent RNA 6000 Nano Kit (Agilent, Santa Clara, USA). 250 ng of total RNA per sample was amplified and labeled using GeneChip®WT PLUS Reagent kit (Affymetrix, Santa Clara, USA) before hybridization over night at 45°C on *GeneChip®Mouse Transcriptome 1.0 Array*. The chip was washed on the GeneChip® Fluidics Station 450 followed by scanning on a GeneChip® Scanner on Affymetrix microarray platform. For quantitative PCR, RNA samples were reversed transcribed using iScript cDNA Synthesis Kit and real time PCR was performed in an iCycler MyIQ2 multicolor-Real-Time PCR detection system using iQ SYBR Green supermix kit (Bio-Rad, Hercules, USA). A standard curve was established for relative quantification with a fourfold dilution series (from 100 to 0.0097 ng) of a cDNA template mix. Relative quantification was calculated by the $2^{\Delta\Delta CT}$ method (*Gapdh* as housekeeping control) and then normalized (percentage or fold) to the control condition (Ct). Primer used (forward/reverse) are :

eNeuro Accepted Manuscript

Gapdh 5'-ACCCAGAAGACTGTGGATGG-3' / 5'- ACACATTGGGGGTAGGAACA-3'

Npas4 5'-GCTATACTCAGAAGGTCCAGAAGGC-3' / 5'-TCAGAGAATGAGGGTAGCACAGC-3'

Egr1 5'-TCCTCTCCATCACATGCCTG-3' / 5'-CACTCTGACACATGCTCCAG-3'

Egr3 5'-GACTCGGTAGCCCATTACAATC-3' / 5'-ACTTTCCCAAGTAGGTCACGG-3'

Western blotting

Cells were solubilized and sonicated in lysis buffer (20% Glycerol, 4% SDS, 125 mM Tris-HCl pH 6.8) containing a cocktail of proteases and phosphatases inhibitors (Roche, Basel, Switzerland). When performed on tissue extracts, mice were euthanized (Ketamine/Xylazine injection) and brains were dissected after perfusion with ice cold sterile PBS. Cortices and hippocampi were isolated and quickly frozen in liquid nitrogen. Tissues were crushed using mortar pestle method. For brain protein extraction, samples were homogenized in RIPA buffer (1% (w/v) NP40, 0.5% (w/v) deoxycholic acid, 0.1% (w/v) SDS, 150 mM NaCl, 1 mM EDTA, 50 mM Tris, pH 7.4) containing proteases and phosphatases inhibitors cocktail. The samples were clarified by centrifugation at 20,000 x g. Protein concentrations were determined with a BCA kit. Samples were prepared with NuPAGE LDS sample buffer (4x) and 50 mM DTT and then heated for 10 min at 70°C. 10 to 40 µg of proteins or 22 µl of culture medium were loaded per well for migration followed by transfer onto PVDF or nitrocellulose membranes. For APP C-terminal fragments, proteins were transferred on nitrocellulose (0.1 µm). Membranes were blocked in nonfat dry milk (5% in PBS, 0.05% Tween-20) and immunoblotted with anti-APP NT (22C11, 1/500), anti-APP CT (Y188, 1/500), anti-APLP1 (1/1000), anti-APLP2 (1/1000) and anti-GAPDH (1/25000). Blots were revealed using ECL and signal quantification was performed using GelQuant.NET software (BiochemLabSolutions.com).

ImmunoCytoFluorescence (ICF)

eNeuro Accepted Manuscript

Neurons grown at 100,000 cells/cm² per well on poly-L-lysine coated coverslips were fixed for 15 min in PBS/4% paraformaldehyde and washed twice in PBS for 5 min. Permeabilization and blocking steps were done in PBS/5% skimmed milk/0.3% Triton-X100. Antibodies were incubated in PBS/5% skimmed milk/0.1% Triton-X100 (M1TPBS). Primary antibodies dilutions used were: mouse anti-MAP2 (1/1000), rabbit anti-APP (Y188, 1/100) and rabbit anti-GAD65 (D5G2, 1/100). Secondary antibodies dilutions used were: goat anti-mouse Alexa Fluor®-488 (1/500), goat anti-mouse Alexa Fluor®-568 (1/500) and goat anti-rabbit Alexa Fluor®-647 (1/500). Images were acquired on Evos FL Auto microscope (Invitrogen) with GFP (Alexa Fluor®-488 or native GFP), TxRed (Alexa Fluor®-568) and CY5 (Alexa Fluor®-647) EVOS LED light cubes and analyzed with ImageJ software. For the quantification of signal area, 10X or 20X magnification images were identically thresholded for APP+/+ and APP-/-, or Ct and CRISPR-*NPAS4*. The area of thresholded images was measured and normalized to the number of cells counted by DAPI staining. For the quantification of the APP expression intensity, image acquisition was performed using 40x objective coverslip-corrected (ThermoFischer Scientific, AMEP4699) in GFP, CY5 (APP) and DAPI channels. A total of 12, 19 and 19 images were acquired and processed to obtain 33, 46 and 51 neurons in the analysis (Figure 3B) for CRISPR control (Ct), Oligo2 and Oligo17 respectively. GFP channel images were first 8-bit transformed and thresholded to highlight only GFP staining. A region of interest (ROI) was delimited around GFP+ neurons in the GFP channel (green) using “wand tool” in imageJ software and transposed to CY5 (APP) channel (blue). ROI mean intensity is measured with the “Analyze” tool of ImageJ software.

AICD and CRISPR/Cas9 lentiviral constructions, production and viral transduction

Lentiviruses were used to express AICD in neurons. AICD50 tagged at the c-terminal part with hemagglutinin (HA) was cloned into pLenti CMV/TO Puro lentiviral vector (Addgene ref #17482). pLenti CMV/TO Puro empty served as a control (Ct). A lentiviral vector-based approach was

eNeuro Accepted Manuscript

also used to deliver the CRISPR-Cas9 system. sgRNAs “Oligo2” and “Oligo17” were designed using on/off-target score algorithm to target the *APP* mouse gene (Gene ID: 11820), and sgRNA “CRISPR-*NPAS4*” to target the *NPAS4* mouse gene (Gene ID: 225872). sgRNAs were cloned in a lentiviral vector delivering sgRNA, SpCas9 and coexpressing eGFP (Addgene #57818) according to author instructions (Heckl et al., 2014). The negative Ct used was the lentiviral construct without sgRNA but expressing SpCas9 and eGFP. sgRNA used are (sequence/PAM/specificity score):

APP Oligo2 5’-GTGGAAGATCCGCCGCGCCC-3’ / TGG / 95

APP Oligo17 5’-GTACCCACTGATGGCAACGC-3’ / CGG / 92

Npas4 5’-GACCCTTGCGAGTGTAGATGC-3 / AGG / 83

All lentiviral vectors were validated by sequencing (Beckman Coulter Genomics, UK) prior to production and purification using the Plasmid Midi kit (Qiagen, Hilden, Germany). Production was carried out by transfecting HEK293-T cells in 10 cm dishes ($2x10^6$ cells/dish) with lentiviral CRISPR-Cas9 vectors, pCMV-dR8.2 (Addgene#12263) and pMD2.G (Addgene#12259). After 48 h, the supernatant was filtered and incubated with 1/3 (v/v) of LentiX™ Concentrator for 90 min on ice. The collected supernatant was centrifuged at 1,500 x g for 45 min at 4°C, the pellet was resuspended in 20 µl per dish of Neurobasal® Medium and stored at -80°C until use.

Neurons were infected with CRISPR-Cas9 lentiviruses 1 day after plating (DIV1). Typically, 20 µl of concentrated virus were used to infect 800,000 cells per well in a 12-well culture dish. The medium was completely changed after 24 hours, and a half-media change was performed every 2-3 days thereafter. The neurons were harvested at DIV7 or as indicated.

Toxicity assay

Cell viability upon lentiviral infection was measured by lactate dehydrogenase (LDH) release in the culture medium using Cytotoxicity Detection kit (Sigma-Aldrich, St-Louis,USA), according to the manufacturer's instructions. Relative absorbance was measured at 490 nm using a VICTOR

eNeuro Accepted Manuscript

Multilabel Plate Reader (PerkinElmer, Richmond, USA). Background LDH release was determined in non-infected control cultures.

Flow cytometry and cell sorting

At DIV7, infected neurons were briefly rinsed with PBS and trypsinized for 2 min. Neurons were mechanically dissociated and filtered through 70 µm Falcon™ Cell Strainers in 50 ml tube containing FBS. Cells were pelleted by centrifugation at 1,000 x g for 5 min and resuspended in PBS/1% FBS/1mM EDTA. TO-PRO™-3 Iodide (Thermo Fisher Scientific, Waltham, USA) was used to stain dead cells and exclude them for the sorting. Cells were sorted using a BD FACSAria™III cell sorter (BD Biosciences, San Jose, USA). The sort parameters used were the following: nozzle 100 µm, sheath pressure 20 psi, drop frequency 30 kHz and sort precision 16-32-0. Sample and collection tubes were maintained at 4°C throughout the procedure. GFP-negative and positive cells were harvested in PBS/1% FBS/1 mM EDTA, centrifuged at 1,2000 x g for 2 min and homogenized in TriPure Isolation Reagent for RNA extraction.

Glutamate and GABA measurements

Neurons were grown at 200,000 cells/cm² in 12 well culture dish. Glutamate and γ-aminobutyric acid (GABA) were measured in cells lysates and culture media at DIV7. Media were harvested, centrifuged to pellet and remove cellular debris, treated with a cocktail of proteases inhibitors and frozen at -20°C until use. Cells were scrapped in ice cold PBS, pelleted by centrifugation (12,000 x g for 3 min at 4°C), quickly frozen in liquid nitrogen and kept at -80°C until use. Glutamate and GABA assays were performed according to the manufacturer's protocol (Abcam, Cambridge, UK). For both, cells were lysed by 5 cycles of thawing and freezing in PBS and centrifuged at 12,000 x g for 10 min at 4°C. Supernatants were used for the quantification and normalized on protein content. Media were directly used for quantification.

Calcium imaging

eNeuro Accepted Manuscript

Changes in intracellular [Ca^{2+}] were measured in single neurons using the calcium sensitive fluorescent dye Fura2 (Molecular Probes, Cambridge, UK). Neurons were grown on poly-L-lysine-coated 15 mm diameter coverslips and were loaded with 2 µM Fura2-acetoxymethyl ester (Fura-2AM) for 40 min in a Krebs buffer (10 mM HEPES, 135 mM NaCl, 6 mM KCl, 2 mM CaCl2, 1.2 mM MgCl2,10 mM glucose, pH 7.4) at room temperature. Coverslips were rinsed once and then mounted on a heated (37°C) and perfused microscope chamber (Warner Instrument Corporation). While continuously perfused with heated Krebs buffer, Fura2-loaded neurons were excited successively at 340 and 380 nm (excitation light was obtained from a xenon lamp coupled to a monochromator) for 2x100 ms. Emitted fluorescence was monitored at 510 nm using a charged coupled device sensor camera coupled to an inverted Olympus IX70 microscope (TILL photonics). Fluorescence intensities from each single neuron was recorded separately, corrected for the background and combined (fluorescence ratio F340/F380) using the software TILLvisION version 3.3. Calcium signals were measured upon application (perfusion) of 30 µM glutamate (Glut) in Krebs buffer. A total of 70–80 cells were analyzed in each experiment (coverslips) and non-neuronal cells were excluded from analysis as previously described by Pickering and coworkers (Pickering et al., 2008). Changes in intracellular [Ca^{2+}] were calculated from fluorescence emission intensity ratios (F340/F380). These changes were expressed as normalized fluorescence where every measurement of F340/F380 was divided by the basal fluorescence value corresponding to the mean of signals measured during a period of 25 s in basal condition (prior to the glutamate stimulation). To estimate the amplitude of the response to glutamate, the area under curve (AUC) was calculated using GraphPad Prism (GraphPad Software, San Diego, USA).

Field potential recordings

3 months old mouse brain slices were prepared as described in (Lepannetier et al., 2018). Excitatory postsynaptic potentials (EPSP) were evoked through a bipolar stimulating electrode

eNeuro Accepted Manuscript

placed in the Schaffer collaterals (SC) and recorded by the AxoClamp 2B (Axon Instruments, USA) amplifier through a glass electrode placed in the CA1 region (stratum radiatum). Stimuli consisted of 100 µs pulses of constant currents with intensity adjusted to produce 35% of the maximum response every min. Responses were digitized by Digidata1322A (Axon Instruments, USA) and recorded to a computer using WinLTP software (Anderson and Collingridge, 2007). Long-term potentiation was induced by applying a theta-burst stimulation (TBS) consisting in four trains of 5 pulses (100 Hz) separated by a 200 ms interval. Slopes of field excitatory postsynaptic potentials (fEPSP) responses were expressed normalized to the pre-treatment baseline, defined as 100%.

Electrophysiology of cultured neurons

Patch-clamp recordings of primary neurons at DIV7 were carried out at room temperature, using an EPC-9 amplifier controlled by PatchMaster software (HEKA Elektronik, Lambrecht, Germany). GABA was applied by pressure ejection using a Picospritzer. The patch pipettes were pulled with a resistance of 4–7 MΩ using a DMZ-Universal Puller (Zeitz Instruments, Munich, Germany). Series resistances were compensated (75–90%) and periodically monitored. The following extracellular solution was used (in mM): 140 NaCl, 5 KCl, 1 $CaCl_2$, 1 $MgCl_2$, 10 glucose, and 10 HEPES, pH 7.4. The pipette solution had the following composition (in mM): 140 CsCl, 10 EGTA, 0.3 Mg2ATP, 0.3 $CaCl_2$, and 10 HEPES, pH 7.25. To prevent network activity, the experiments were performed in the presence of 1 µM tetrodotoxin (TTX), 10 µM 6-cyano-7-nitroquinoxaline-2,3-dione disodium (CNQX) and 20 µM D-(-)-2-Amino-5-phosphonopentanoic acid (D-AP5) and 100 nM CGP55845.

Statistical analysis

Microarray analysis: Raw data were analyzed using Bioconductor (R environment). Robust Multiarray Average (RMA) was used for background correction, normalization, probe level

eNeuro Accepted Manuscript

intensity calculation and probe set summarization. Gene expression values were compared between APP+/+ and APP-/- neurons at different stage of development DIV3, DIV7 and E18 using the R-Limma (Linear Models for MicroArray Data) package. Benjamini-Hochberg procedure was used for multiple testing corrections. Only transcripts with an Entrez ID were kept among the raw data in order to facilitate the analysis. Gene set enrichment analysis was performed on differentially expressed genes sets after the ROAST (Rotation gene set tests for complex microarray experiments) (Wu et al., 2010) procedure to identify KEGG pathways modified in absence of APP for all conditions (E18, DIV3 and DIV7). The data obtained have been deposited in NCBI's Gene Expression Omnibus (Edgar et al., 2002) and are accessible through GEO Series. Otherwise, statistical analyses were performed using GraphPad Prism (GraphPad Software, San Diego, USA). Gaussian distribution was assessed by Kolmogorov-Smirnov test (GraphPad Prism). Parametric test was applied if the data followed normal distribution. Otherwise non-parametric tests were used. When two groups were compared, parametric Student's t-test or non-parametric Mann-Whitney test were used. When more than two groups were compared, parametric ANOVA with indicated post hoc tests or non-parametric Kruskall-Wallis were used. Significance is indicated as ns = non-significant; * $p < 0.05$; ** $p < 0.01$; *** $p < 0.001$. The number of samples per condition in one experiment (n) and the number of biological replicates (N) are indicated in figure legends.

eNeuro Accepted Manuscript

Results

APP-dependent expression of NPAS4 in differentiated primary neuron cultures

Transcriptome analysis were performed on primary neurons and embryonic cortex according to the workflow described in Extended Data Fig. 1-1A. Neurons from embryonic cortex (E18) were cultured for 3 or 7 days in vitro (DIV3 or DIV7) and up to DIV14 when necessary. Characterization of APP protein family expression indicated an increase in APP, APLP1 and APLP2 upon differentiation with a peak of expression at DIV7-8 (Extended Data Fig. 1-1B-C), supporting an important role of APP protein family in neuronal maturation. APLP1 and APLP2 levels were similar in APP-/- neurons and APP+/+ at any time point of differentiation (Extended Data Fig. 1-1D). Thus, the results obtained here in APP-/- neurons are related to the loss of APP and not to indirect effects resulting from up- or down-regulation of APLP1 or APLP2 in the absence of APP.

Previous studies indicated that APP-dependent gene transcription involves the release of its intracellular domain or AICD. AICD is detectable in the nucleus of primary neurons at DIV6-7 (Kimberly et al., 2005), suggesting that AICD-dependent gene transcription should be temporally restricted. We monitored AICD production at DIV7 in APP+/+, APP+/- and APP-/- cultures (Extended Data Fig. 1-1E). AICD was only readily detectable in APP+/+ neurons at a high exposure time, confirming (i) that it is a transient peptide (Huysseune et al., 2007) with a restricted temporally expression pattern in primary neurons and (ii) that APP-dependent transcriptional regulation may occur at a defined time-period (around DIV7). We thus performed microarray experiments at several differentiation stages (summarized in Extended Data Fig. 1-1A) to track genome-wide expression changes in APP +/+ and APP-/- primary cortical neurons at DIV3 (immature neuronal network, no AICD), DIV7 (neuronal network with detectable AICD) and in E18 cortical tissue (embryonic tissue). We used *Affymetrix GeneChip®Mouse Transcriptome 1.0 Array* and performed data analysis with the R-Limma (**Li**near **M**odels for

eNeuro Accepted Manuscript

Micro**A**rray Data) package (Ritchie et al., 2015). The chips used allowed profiling of the expression of coding and non-coding genes (lncRNA, miRNA, pseudogene…) as well as alternative splicing events. Transcriptome analysis was performed in triplicate (N=3 independent cultures) for each condition (E18, DIV3, and DIV7). We focused on differentially expressed coding genes, although data were also collected for non-coding RNAs. Strikingly, the overall changes observed (fold changes) were moderate in all conditions (E18, DIV3 and DIV7). Few coding transcripts appear to be differentially expressed when the specific fold change (linear) is set at 1.25, 1.5 or 2 (Fig. 1A). The Benjamini-Hochberg multiple correction test did not reveal any robust differential gene expression (adjusted p-value <0.05) excepted for *APP* (positive control). To note, we did not measure significant change in the expression of genes previously identified as AICD target genes (Pardossi-Piquard and Checler, 2012). Gene enrichment analysis was further performed using the ROAST (Rotation gene set test for complex microarray experiment) procedure to identify a molecular interaction/reaction networks diagram known as the KEGG pathway (Kanehisa and Goto, 2000) altered in the absence of APP. The first five pathways (in terms of significance), the number of genes modified as well as their direction are shown in Fig. 1B. For instance, *ECM (extracellular matrix)-receptor interaction* and *Long-term potentiation* pathways appeared to be modulated in absence of APP at DIV7. APP shares the structure of transmembrane receptors and cell adhesion proteins that activate Cell-ECM pathways. Long term potentiation (LTP) is a major mechanism in memory formation and learning. Both of these pathways have been associated to APP function (Caceres and Brandan, 1997; Seabrook et al., 1999; Puzzo et al., 2011). We kept this pathways analysis to further investigate the regulation of candidate genes relevant to APP functions. In a set of arrays from a primary neuron at DIV7 (APP+/+ vs APP-/-), we noticed a down-regulation of Inducible Transcription Factors (ITFs) or Immediate Early Genes (IEGs) in APP-/- neurons (Fig. 1C). Among them, the activity-dependent transcription factor NPAS4 (Neuronal PAS domain protein 4). NPAS4 is a neuron-specific ITF, known to be regulated by neuronal depolarization. We

eNeuro Accepted Manuscript

confirmed by qPCR that the NPAS4 mRNA level was decreased at DIV7 in APP-/- neurons, but neither at DIV3 nor in the cortex at E18 (Fig. 1D). To note, the expression of other IEGs (*Egr1* and *Egr3*) previously reported to be APP downstream targets (Hendrickx et al., 2013;Hendrickx et al., 2014) was not altered in our experiments (See Extended Data Fig. 1-2).

Control of NPAS4 expression by APP

Since AICD - produced at DIV7 – is reported to mediate APP nuclear signaling (Belyaev et al., 2010), we analyzed its involvement in NPAS4 expression. We transduced primary neurons with a lentiviral vector expressing the 50 C-terminal amino acids of APP (AICD) fused at the C-terminus to the hemagglutinin tag (HA). AICD-HA is detectable in infected cells (Fig. 2A) and AICD expression in APP-/- neurons significantly increased NPAS4 mRNA levels (Fig. 2B), indicating that AICD is involved in the transcriptional regulation of NPAS4. As some of the APP functions were found to rely on its extracellular soluble fragment (sAPPα), we tested whether the sAPPα can regulate NPAS4 expression *per se*. Treatment of neuronal cultures with 20 nM of human sAPPα (Fig. 2C) significantly increased NPAS4 mRNA levels in APP+/+ neurons, but not in APP-/- neurons (Fig. 2D). Together, these data indicate that (i) AICD is likely to be involved in APP-dependent NPAS4 transcription (ii) soluble APP (sAPPα) triggers NPAS4 expression, but only in a context where endogenous APP is expressed. Importantly, glial cells (about ~16% of total cells in primary cultures) could indirectly contribute to these observations. We found that the absence of APP did not change the astrocytic pattern of primary cultures, and that astrocytes did not readily express NPAS4 in contrast to neuron (Extended Data Fig. 2-1). Moreover, NPAS4 is strongly induced as expected by depolarization only in neurons (Sun and Lin, 2016). Together, this indicated that NPAS4 is a downstream transcriptional target that could be involved in APP neuronal functions.

The mild APP-dependent transcriptional regulations we observed are in line with the mild phenotype of APP knockout mice (Muller et al., 1994; Zheng et al., 1995). Still, APP-dependent

eNeuro Accepted Manuscript

gene regulations that occur in the close-up could be hidden in the long term by functional redundancies with other members of the APP family (Shariati and De Strooper, 2013). In agreement, APP-/- phenotype is better unraveled by acute down-regulation of APP in the brain (Senechal et al., 2007). We performed a knockdown of APP expression in neurons with a lentiviral-based CRISPR-Cas9 genome editing approach (Jinek et al., 2012) to test the consequence of acute APP downregulation on NPAS4 expression. Nearly ~50% of the cells were infected and no lentiviral toxicity was measured under our conditions (Extended Data Fig. 3-1). Only neuronal cells were infected, reflecting the tropism of the viral particles for neurons. APP expression was analyzed by ICF (Fig. 3A). Measurement of the intensity of APP signal in infected (GFP-positive) neurons (Fig. 3B) indicated a strong decrease in APP expression (40 to 50%) in neurons infected with CRISPR-Cas9 viruses targeting APP exon1 and exon 2 (Oligo2 and 17 sgRNA, respectively). This was confirmed by Western blotting (Fig. 3C). Importantly, expression of APLP1 and APLP2 was not altered in neurons infected under the same conditions, indicating that off target editing of APP did not occur in our experimental setup. To measure the expression of NPAS4 selectively in GFP-positive (knockdown) neurons, we sorted GFP positive neurons by flow cytometry (Fig. 3D). TO-PRO™-3 staining was used as a viability marker to exclude dead cells from the analysis. The sorting parameters were set by using non-infected neurons (GFP negative) and neurons expressing GFP (GFP positive) as standards. NPAS4 mRNA was readily decreased in neurons infected with Oligo2- and 17-expressing lentiviruses (GFP positive). Thus, acute APP knockdown resulted in decreased NPAS4 mRNA levels, confirming the APP-dependent NPAS4 transcriptional regulation observed in APP-/- neurons.

APP deficiency increases markers associated to GABAergic transmission

NPAS4 is an ITF induced by neuronal activity. The down-regulation of NPAS4 expression observed in the absence of APP could reflect an impairment in the establishment of a functional network, leading to defects in basal neuronal activity. APP was reported to modulate neurite

eNeuro Accepted Manuscript

517 outgrowth and synapse formation (Priller et al., 2006; Young-Pearse et al., 2007; Tyan et al.,
518 2012; Billnitzer et al., 2013). We analyzed neuronal arborization by measuring the area of the
519 neuron-specific microtubule associated protein2 (MAP2) signal per cell from DIV1 to DIV7 (Fig.
520 4). Neurite extension observed in APP+/+ and APP-/- neurons was not significantly different at
521 DIV1 and DIV3. Strikingly, the absence of APP significantly increased MAP2 signal at DIV7,
522 indicating the importance of APP for in neurite arborization and formation of a functional
523 network. This observation reinforced the possible involvement of NPAS4 in APP physiological
524 function. NPAS4 activity scales the neuronal network by controlling the balance of excitatory and
525 inhibitory inputs on post-synaptic neurons (Lin et al., 2008; Bloodgood et al., 2013; Spiegel et al.,
526 2014). We measured the amount of two neuromediators, GABA (released at inhibitory
527 synapses) and glutamate (released at excitatory synapses) in the medium and in the cells of
528 primary neurons at DIV7 (Fig. 5A-B). The concentration of GABA was increased by 83% in the
529 medium of APP-/- neurons (Fig. 5A). No significant change in glutamate concentration (cell or
530 medium) was observed in APP-/- neuronal cultures when compared to APP+/+ (Fig. 5B). In line
531 with this observation, we measured only very subtle changes in glutamate responses in APP-/-
532 neurons when compared to APP+/+ (Extended Data Fig. 5-1), pointing toward a specific
533 impairment in GABA-dependent signaling in the absence of APP. GABA is synthetized in
534 inhibitory neurons by the glutamate decarboxylase enzymes (GAD_{65} and GAD_{67}). GAD_{65} is
535 active at nerve terminals and synapses. We observed that GAD_{65} signal is increased in APP-/-
536 neurons when compared to APP+/+ (Fig. 5C). This is not caused by an increase in the relative
537 number of GAD_{65} positive neurons in APP-/- cultures (Extended Data Fig. 5-2), but likely to an
538 increase in GAD65 expression in GABAergic neurons. To further address the effect of APP
539 deficiency on GABAergic synaptic markers, we first quantified the expression of GABARα1, a
540 $GABA_A$ receptor subunit predominantly expressed during neuronal development. We found a
541 slight but significant decrease in GABARα1 in APP-/- neurons (Fig. 5D). To evaluate if the
542 activity of GABA receptors was defective in physiological conditions, cortical neurons at DIV7

eNeuro Accepted Manuscript

were voltage-clamped at -60mV. To prevent neuronal activity, experiments were performed in the presence of 1 µM TTX, 10 µM CNQX, 20 µM D-AP5 and 100 nM CGP55845 to inhibit Na^+ voltage-dependent channels, AMPA, NMDA and $GABA_B$ receptors, respectively. Current-voltage (IV) curves were generated by evoking the current with a voltage ramp stimulus from -90mV to +60mV, and the response to 100 µM was studied (Fig. 5E). Whole cell currents evoked at -50mV or +50mV by 100µM GABA were similar in APP+/+ as in APP-/- neurons (Fig. 5F). This patch-clamp investigation did thus not reveal any functional decrease in $GABA_A$ receptors, suggesting that the minor decrease in expression of GABARα1 subunit was compensated.

Finally, we evaluated the impairment in GABAergic markers in the brain of APP-/- mice. We quantified the expression of GAD65 and GABARα1 in cortices and hippocampi of 3-month-old mice. A significant increase in GAD65 expression was observed both in cortex (Figure 6A) and in hippocampus (Figure 6B) of APP-/- mice, and decreased GABARα1 levels were measured especially in the hippocampus. We analyzed CA3-to-CA1 synapse plasticity by extracellular recordings on hippocampal slices from adult APP+/+ and APP-/- mice. Schaffer collaterals (SC) were stimulated and fEPSP were recorded in the stratum radiatum of CA1 region. We observed that the relationship between the stimulus intensity and the fEPSP slope was similar in slices from both genotypes (Extended Data Fig. 6-1A). To investigate LTP, we stimulated the SC pathway with a theta- burst stimulation (TBS) consisting of four bursts of five pulses (given at 100 Hz) separated by 200 ms. In slices from APP+/+ animals, TBS induced a large increase of the fEPSP response size that decayed over the first 20 minutes to a plateau level persisting up to the end of the experiment. In APP-/- mice, LTP was significantly reduced (Fig. 6C). Typically, 60 min after the TBS, LTP was reduced by half. The response to TBS itself was actually modified: the second, third and fourth bursts of stimulation were globally decreased in APP-/- compared to APP+/+, and within each of the four bursts of 5 pulses, the responses to the third, fourth and fifth stimuli decreased more in slices form APP-/- mice than in APP+/+ (Fig. 6D).

eNeuro Accepted Manuscript

568

569

570 **Silencing NPAS4 mimics APP deficiency in neurons**

571 We used the CRISPR-Cas9 approach in order to directly silence *NPAS4* expression in neurons
572 and analyze whether NPAS4 deficiency could recapitulate a major trait observed in APP-/-
573 neurons, i.e. the upregulation of GABA release and modification of GABAergic markers. The
574 efficiency of CRISPR-Cas9 editing is hard to evaluate by quantifying the mRNA levels of the
575 target gene, since decrease in mRNA could only occur if nucleotide insertions by non-
576 homologous end-joining results in nonsense-mediated RNA decay. Commercially available
577 antibodies poorly detect NPAS4 in basal conditions, but we could still observe that NPAS4
578 protein was diminished upon silencing (CRISPR-*NPAS4* condition, Fig. 7A). We further decided
579 to check the down-regulation of *NPAS4* gene expression by measuring NPAS4 protein upon
580 depolarization by KCl (Lin et al., 2008). In that condition, we found that CRISPR-Cas9-induced
581 silencing resulted in a decrease in NPAS4 by approximately 50% (Fig. 7A). This is comparable
582 to the decrease in NPAS4 mRNAs measured in APP-/- neurons at DIV7 (Fig. 1D). As for
583 CRISPR-Cas9 lentiviral vectors targeting APP, we did not observe toxic effects related to viral
584 transduction of primary neurons (See Extended Data Fig. 3-1C). Strikingly, like APP-deficient
585 primary neurons (Fig. 5C) or brains of APP-/- mice (Fig.6), NPAS4-deficient neurons showed an
586 increase in GAD65 staining (Fig. 7B-C) and GAD65 protein expression (Fig. 7D). Accordingly, a
587 2.5-fold increase in GABA concentration was measured in the medium of primary neurons
588 infected with CRISPR-Cas9 *NPAS4* lentiviruses (Fig. 7C). The expression of GABA receptor
589 subunit alpha 1 (GABARa1) was decreased after *NPAS4* knockdown (Fig.7D), to the same
590 extent as the decrease observed in in APP-/- primary neurons (Fig. 5D).

591

eNeuro Accepted Manuscript

Discussion

One major function of APP is to control synaptic formation, transmission and plasticity (Muller et al., 2017). We showed here that APP deficiency in cortical neurons impairs the balance between excitatory and inhibitory synaptic markers, and increases GABAergic transmission. This process relies on the activity-dependent transcription factor NPAS4. We initially identified the NPAS4 IEG as downstream APP target by a non-biased transcriptome analysis. The APP-dependent transcription of NPAS4 involves its extracellular domain (sAPPα) and is activated by AICD. APP appears thus to exert a fine tuning of inhibitory synapses in neuronal network. Its absence enhances, through the downregulation of NPAS4, the production and the release of GABA.

APP-dependent expression of NPAS4 in differentiated neurons

The transcriptome analysis of APP+/+ vs. APP-/- neurons at embryonic day 18 (E18-DIV0) and at different stages of primary cortical neuron differentiation (DIV3-DIV7) indicated that the transcriptional changes in the absence of APP were moderate. This unexpected result is in line with a comparative transcriptome study of APP family members in the adult mouse cortex (Aydin et al., 2011). Subtle effects of APP deficiency on the transcriptome could be due to functional redundancies with other APLPs that display similar functions and signaling properties (Shariati and De Strooper, 2013). We did not measure any changes in APLP1 and APLP2 expression in our APP-/- models, in agreement with studies done on total brain extracts (Zheng et al., 1995) or in primary cortical neurons (White et al., 1998). Transcriptional modifications we measured are thus related to the absence of the APP protein *per se*. APP-dependent transcriptional regulations likely act by fine-tuning the expression of classes of gene involved in neuronal pathways rather than robustly regulating single target genes. We found that the expression of the NPAS4 ITF is downregulated in the absence of APP. This particularly at DIV7, when primary neurons start to form a functional network. NPAS4 downregulation was observed it in APP-/- primary neurons and upon acute APP knockdown by a CRISPR-Cas9 approach, establishing a

eNeuro Accepted Manuscript

link between APP and NPAS4 transcription. Regarding the possible molecular mechanisms involved here in APP-dependent gene transcription, we found that NPAS4 expression is activated in neurons by AICD expression. It correlates with the fact that DIV7 corresponds to the differentiation stage where AICD is peaking in primary cortical neurons. (Kimberly et al., 2005). However, previous studies showed the secreted ectodomain (sAPPα) is sufficient to rescue functional defects in APP KO mice (Ring et al., 2007; Weyer et al., 2014). We found that treatment of APP+/+ neurons (and not APP-/- neurons) with sAPPα significantly increased NPAS4 mRNAs. This observation indicates that (i) the effects of sAPPα require the presence of endogenous APP (ii) homophilic ectodomain interactions are likely to be involved. Soluble APP was suggested to promote its physiological effects by interaction with APP holoprotein (Milosch et al., 2014; Deyts et al., 2016). It is tempting to suggest here that interaction of soluble APP with APP holoprotein present at the cell surface could induce the release of transcriptionally active AICD, but this hypothesis awaits further experimental evidence.

Alteration of GABA release and GABA markers in APP deficient neurons

In the absence of APP, we observed an increase in neuronal outgrowth and GAD65 signal, as well as increased GABA release in the medium of primary neurons. The increase in GAD65 signal was related to an increased signal in GAD65-positive neurons, not to an increased number of GAD65 neurons in our primary cultures. It would be useful to further investigate as to whether an increase in the numbers and functionality of GABAergic neurons occurs in the brain of APP -/- mice. To note, APP was reported to control neurogenesis in adult mice brain (Wang et al., 2014), as process that could account for the modification of neuronal subtypes observed in the absence of APP.

The increase-in GAD65 we observed was in line with increased levels of GABA in the culture medium. *In vivo* studies evidenced increased GABA levels in the brain of APP-/- mice (Lee et al., 2010). However, this elevation of GABA markers was concomitant to a down-regulation in the

eNeuro Accepted Manuscript

642 GABARα1 receptor subunit. Recent study also reported that GABARα1 is particularly decreased
643 in hippocampus of APP-/- mice (Chen et al., 2017), in line with our in vivo experiments. Still,
644 patch-clamp experiments did not reveal any decrease in $GABA_A$ receptors functionality,
645 indicating that compensation may occur to circumvent the decrease in a $GABA_A$ receptor
646 subunit, and that GABAergic transmission per se is not significantly altered.

647 On the other hand, our results show that LTP is reduced in brain slices from APP-/- mice. This is
648 in agreement with previous studies showing that the LTP induced by one TBS is reduced in
649 APP-/- at the SC-CA1 synapses (Dawson et al., 1999;Seabrook et al., 1999;Ring et al., 2007)
650 but not at the perforant path-granule cell (DG) synapse that we did not study here (Jedlicka et
651 al., 2012), Such inhibition was however not observed by other investigators (Wang et al., 2017),
652 possibly because they used a stronger stimulation protocol (3 TBS). Interestingly, the analysis of
653 the responses to the TBS itself is consistent with increased GABAergic release in APP-/- mice.

654 How could APP modulate GABA release? Soluble APP (sAPPα) is known to enhance LTP and it
655 is sufficient to rescue the decrease of LTP observed in APP-/- mice (Taylor et al., 2008;Ring et
656 al., 2007). Moreover, very recent studies showed that the sAPPα directly binds the $GABA_B$
657 receptor subunit 1a (GABABR1a), suppressing synaptic transmission and triggering short-term
658 facilitation in hippocampal neurons (Rice et al., 2019). Such an effect of sAPPα could explain the
659 smaller response observed in brain slices from APP-/- mice compared to APP+/+. Indeed, in
660 APP-/- slices, a larger release of GABA would occur in the absence of $GABA_B$R1a stimulation by
661 sAPPα, therefore reducing the disinhibitory process observed between the first and the second
662 burst of stimuli of the TBS (Larson and Munkacsy, 2015). This supports that APP synaptic
663 function and APP-dependent synaptic transmission are mediated by the soluble sAPPα
664 fragment. We suggest that the NPAS4 IEG is sensing the APP-dependent modulations of
665 synaptic transmission. Our results also indicate that NPAS4 knockdown mimics APP deficiency
666 on GAD65 levels and GABA measurements. The finding that APP functions in neuronal network

eNeuro Accepted Manuscript

might be mediated by NPAS4 is relevant to several evidences about the reported role of NPAS4 in neuronal network activity. NPAS4 possesses unique features among the IEGs (Sun and Lin, 2016): (i) it is only expressed in neurons; (ii) it is activated selectively by neuronal activity; (iii) it has been shown to shape glutamatergic and GABAergic synaptic inputs. NPAS4 is implicated in a transcriptional program that regulates neuronal firing responses to excitatory transmission by enhancing inhibition (Lin et al., 2008), and is critical to keep neuronal firing in response to stimuli within normal levels (Spiegel et al., 2014). This exciting new field of investigation connecting APP function to ITFs sensing neuronal activity awaits further investigation.

Possible relevance to the AD pathophysiology

APP plays a central role in the onset and progression of the amyloid pathology found in AD. Apart from producing Aβ, the precise contribution of the APP protein to the pathology is poorly understood. The impairment of APP function, either caused by Familial AD (FAD) mutations or upon neuronal ageing, may contribute to neuronal dysfunctions occurring in the disease. In the mammalian brain, APP modulates dendritic complexity, synaptic functions and synaptic plasticity (Muller et al., 2017). A reduction in dendritic length and branching as well as in total spine density was reported in old APP-deficient mice (Lee et al., 2010; Tyan et al., 2012). Aging is an important parameter related to APP functions in the brain. The phenotype related to APP deletion in the central nervous system (CNS) is age-dependent (Priller et al., 2006). Upon aging, impairments in learning and memory associated with deficits in LTP are observed in APP-deficient mice as shown here and in previous studies (Ring et al., 2007). Interestingly, the decline in memory performance and reduction in LTP observed in old mice and APP transgenic mice are mediated by the ionotropic $GABA_A$ receptor (Yoshiike et al., 2008). This imbalance in neuronal excitatory/inhibitory transmission was also observed in the temporal cortex of AD patients, where significantly lower levels of GABA and glutamate were measured (Gueli and Taibi, 2013). These observations unambiguously indicate that changes in neurotransmission

eNeuro Accepted Manuscript

692 occur in AD (and even in ageing brain) and point toward alteration of the inhibitory GABAergic
693 transmission. Important points must be kept in mind here. First, GABAergic transmission shifts
694 from excitatory to inhibitory during development (Ben-Ari, 2002), so the consequence of altered
695 GABAergic transmission can be fully understood only in adult brain. Then, the molecular
696 mechanisms underlying changes in inhibitory transmission in AD are complex. The GABAergic
697 molecular actors are differentially affected by ageing (Vela et al., 2003) or in AD mice models
698 (Yoshiike et al., 2008). Decrease in GABARα1 has been reported in ageing rodent brain and in
699 the hippocampus of aged brains with AD (Mizukami et al., 1998), but this could be functionally
700 compensated as shown herein. Our findings should further be addressed in AD mice models
701 (expressing APP mutations) to complete the results obtained here in a loss-of-function model
702 (APPKO). However, the hypothesis of an overall impairment of GABAergic transmission in AD is
703 also supported by the increased risk for unprovoked seizures observed in individuals with AD
704 compared to non-demented individuals of the same age (Friedman et al., 2012).

705 Finally, NPAS4 expression was found to decrease along with AD progression, particularly at
706 Braak NFT stages (I-II) corresponding to lesions developed in transentorhinal/entorhinal cortex
707 (Miyashita et al., 2014). We believe that our main observation, namely that APP deficiency in
708 neurons is integrated by the activity-dependent NPAS4 IEG and affects the balance of inhibitory
709 and excitatory neuronal inputs, provides new insight to understand the role of APP in synaptic
710 activity, but also a mechanistic frame to further explore the impairments of network activity in
711 AD.

712

eNeuro Accepted Manuscript

Figure Legends

Figure 1: APP-dependent expression of NPAS4 in young differentiating neuronal culture

Summary of transcriptome analysis performed with the *GeneChip® Mouse Transcriptome Array 1.0* (Affymetrix). The characterization of the model and the experimental workflow are described in Extended Data Fig. 1-1. Data were processed in triplicate (N=3) for each experimental time point (E18; DIV3; DIV7). Non-coding transcripts and alternative splicing products were detected by these arrays, but only transcripts of coding transcripts have been considered here. For all the transcripts, adjusted p-value > 0.05 except for APP (internal control, p-value < 0.05). **A**) Number of up-and down-regulated coding transcript in APP-/- vs. APP+/+ primary neurons at E18, DIV3 and DIV7. Linear fold changes have been set at 1.25, 1.5 and 2. **B**) KEGG pathway analysis (http://www.genome.jp/kegg/pathway.html) at E18, DIV3, DIV7 (APP-/- vs. APP+/+) to identify networks molecular pathways (or interaction networks) in which differentially expressed genes are clustered. The five most modified pathways are displayed for each time point, with the number of genes potentially up-or down-regulated. **C**) Immediate Early Genes (IEGs) expression in APP-/- vs. APP+/+ primary neurons at DIV7 and their respective fold change (APP-/- vs APP+/+) in microarray analysis at DIV7. **D**) Neuronal PAS 4 domain (*NPAS4*) mRNA level was measured by qPCR at E18, DIV3 and DIV7 (n=6, N=3). Results (mean ± SEM) are expressed as percentage of controls (APP+/+). n.s.= non-significant, *p=0.0242, Student's t-test. mRNA levels of two other IEGs (Egr1 and Egr3) were measured in the same conditions (Extended Data Fig. 1-2).

Figure 2: APP metabolites regulate NPAS4 expression

A) Schematic representation of APP, its fragments, the AICD-HA construct along with and the localization of the epitopes recognized by the different antibodies used. Western blotting analysis of AICD-HA expression after 3 days of lentiviral infection in cells with control or AICD-

eNeuro Accepted Manuscript

HA expressing vectors. Total cell lysate was analyzed with anti-HA antibody. **B**) Quantification by qPCR of NPAS4 mRNA in neurons APP-/- at DIV7 infected with lentiviral vector expressing AICD-HA (n=6, N=3). Results are expressed as percentage of control (Ct) (mean± s.e.m). *p.= 0.0291, Student-t test. **C**) Medium of sAPPα treated APP+/+ or APP-/- neurons was subjected to Western blotting analysis using anti-human APP antibody (clone W0-2) to detect the exogenous human sAPPα (h sAPPα) and an anti-mouse APP antibody (clone 22C11) to detect both endogenous and exogenous sAPPα (h+m sAPPα). Medium was collected after 16 h of treatment. **D**) Quantification by qPCR of NPAS4 mRNA level in APP+/+ (n=8, N=4) or in APP-/- neurons at DIV7 treated with 20 nM sAPPα for 16 h (n=6, N=3). Results are expressed as percentage of control (Ct) (mean ± s.e.m.). **p=0.0055, n.s.= non-significant, Student-t test. Given that primary cultures of cortical neurons at DIV 7 also contain astrocytes, the astrocytic pattern of NPAS4 expression is described in Extended Data Fig. 2-1.

Figure 3: Decreased NPAS4 expression in APP-silenced primary neurons

APP was knockdown by CRISPR-Cas9 approach in primary neurons cultures. The infectivity and toxicity of lentiviral CRISPR-Cas9 vectors are detailed in Extended Data Fig. 3-1. **A**) APP expression characterization in neurons by immunostaining. Cortical neurons were infected at DIV1 with lentiviruses expressing sgRNAs (Oligo2, Oligo17) or not (Ct). All lentiviruses harbor a GFP expression cassette. Cultures were immunostained for MAP2 (red), APP (blue) and DAPI (light blue) at DIV7. Arrowheads indicate the position of GFP-positive (infected) neurons in each condition. Scale bar: 100µm. **B**) Quantification of APP signal in GFP-positive neurons by Image-J. At least 33 neurons were quantified in two independent experiments for each condition (n=33 N=2). Results (mean ± SEM) are given as percentage of control (Ct). ###p<0,001 (Ct vs Oligo 2) ***p<0.001 (Ct vs Oligo17); Kruskal-Wallis test and Dunn's multiple comparison test. **C**) Upper panel. Representative Western blots showing APP, APLP1, APLP2 and GAPDH protein levels in cortical neurons at DIV7 infected in the same conditions as in Fig 1A. NI = non-infected. Lower

eNeuro Accepted Manuscript

762 panel. Quantification of APP expression in total cell lysates measured by Western blotting.
763 Results (mean ± SEM) are given as percentage of control (Ct). ***p<0,001 (Ct vs Oligo17),
764 ###p<0.001 (Ct vs Oligo 2), ANOVA and Bonferroni's multiple comparison test (n=6, N=3). **D**)
765 Sorting of GFP-expressing neurons (FACS). Scatter plots (FSC vs. SSC, left panels) of non-
766 infected and GFP-expressing cells are shown. Dot plots (TOPRO-3, far red vs. GFP, right
767 panels) were used to gate (green rectangle) GFP-positive/TOPRO-3 negative cells. RNA was
768 extracted from these cells and NPAS4 mRNA level was quantified by qPCR. Results were
769 obtained from pooled samples (4 wells of 4 cm^2 each) for each condition (Ct, Oligo2 and
770 Oligo17). Quantification was carried out on 2 independent experiments (N=2). Results (mean ±
771 SEM) are expressed as percentage of Ct.

772 **Figure 4: Altered neurites arborization of APP deficient neurons during in vitro maturation**

773 **A**) Cortical APP+/+ or APP-/- were stained against the neuron-specific marker MAP2 and the
774 nuclear dye DAPI at different stages of maturation (DIV1-2-3 and DIV7). Scale bar: 400µm. **B**)
775 Quantification by ImageJ of MAP2 signal area normalized to the number of neurons at DIV1, 2, 3
776 and 7. Quantifications were from 3 fields of at least 6 coverslips from APP+/+ and APP-/-
777 neurons, in three independent experiments (N=3). Results (mean ± SEM) are expressed as
778 percentage of control (APP+/+). *p=0.0293, Mann-Whitney test.

779 **Figure 5: GABAergic markers and GABAergic transmission in APP knockout neurons**

780 **A**) Quantification of γ-amino butyric acid (GABA) in culture medium and cell extracts of APP+/+
781 and APP-/- primary neurons at DIV7. Results (mean ± SEM) are expressed as percentage of
782 APP+/+ (n=20, N=3). **p=0.0024, n.s.= non-significant, Student-t test. **B**) Quantification of
783 glutamate in culture medium and cell extracts of APP+/+ and APP-/- neurons at DIV7. Results
784 (mean ± SEM) are expressed as percentage of APP+/+ (n=16, N=3). n.s.= non-significant,
785 Student-t test. Glutamate responses measured in APP-/- neurons are shown in Extended Data

eNeuro Accepted Manuscript

Fig. 5-1. **C**) Cortical APP+/+ and APP-/- neurons at DIV7 were immunostained for the neuron-specific marker MAP2 and glutamate decarboxylase 65 (GAD65). Arrows indicate MAP2/GAD65 positive neurons, shown at higher magnification (insets). The expression profile of the GAD65 GABAergic marker in APP+/+ and APP-/- neurons is detailed in Extended Data Fig. 5-2. GAD65 signal (5 fields per coverslip) was normalized for quantification to the number of cells in the area (histogram on the right). At least 2 coverslips were quantified for each group (APP+/+ and APP-/-) in two independent experiments (N=2). Results (mean ± SEM) are given as percentage of control (APP+/+). Scale bar: 200µm. *p=0.0220, Mann-Whitney test. **D)** Neurons harvested at DIV7 and cell extracts analyzed by Western blotting for GABARα1 and GADPH expression. Quantification of GABARα1 was normalized to GAPDH expression. Results (mean ± SEM) are expressed as percentage of Ct (n=5, N=2). *p=0.0197, Student's t-test. **E)** Representative I-V traces (from −90 to +60 mV repeated every 0.1 s) through APP+/+ (A) and APP-/- (B) neurons, in the presence 100 µM GABA (red traces). **F)** Pooled data of whole-cell current (at +50 and -50 mV) evoked by 100 mM GABA, through APP WT and KO neurons. Each column represents mean ± SEM of n=8 cells.

Figure 6: GABAergic markers and LTP in adult mice

A) *Left panel:* Western blot analysis of GAD65, GABARα1 and GAPDH expression in cortex of 3 month old APP+/+ and APP-/- mice (N=5). *Right panel:* Quantification of GAD65 and GABARα1 were normalized to GAPDH expression. Results (mean ± SEM) are expressed as percentage of APP+/+ (N=5). *p=0.0166, Student's t-test. **B**) *Left panel* Western blot analysis of GAD65, GABARα1 and GAPDH expression in hippocampus of 3 month old APP+/+ and APP-/- mice (N=5). *Right panel* Quantification of GAD65 and GABARα1 were normalized to GAPDH expression. Results (mean ± SEM) are expressed as percentage of APP+/+ (N=5). *p=0.0404, Student's t-test. LTP was measured in hippocampal SC-CA1 pathway from APP+/+ (n=9) and APP-/- mice (n=8). The input-output relationship between fEPSP measured in CA1 stratum

eNeuro Accepted Manuscript

radiatum and the intensity of SC stimulation is depicted in Extended Data Fig. 6-1. **C**) fEPSP slopes measured during TBS ($p<0.05$; two-way repeated measurements ANOVA, Bonferroni). **D**) fEPSP slopes measured before and after TBS. Results expressed in proportion of the baseline response (100%). ($p<0.05$; two way repeated measurements ANOVA, Bonferroni).

Figure 7: NPAS4 silencing by CRISPR-Cas9 mimics cell phenotype observed in APP deficient neurons.

Changes on inhibitory (GABA) synapses was analyzed after *NPAS4* silencing **A**) *Left panel.* Cortical neurons infected with CRISPR-Cas9 lentivirus targeting *NPAS4* gene (CRISPR-*NPAS4*) show reduced NPAS4 levels as measured by Western blotting (high exposure). Same experiments were carried out after membrane depolarization with 50mM potassium chloride (KCl). NPAS4 accumulations was detectable by Western blotting at low exposure. Viruses without sgRNA were used as controls (Ct). *Right panel.* Quantification of NPAS4 protein level after 2, 3 and 4h of KCl depolarization. Results (mean ± SEM) are expressed as percentage of non-treated controls Ct (N=2). ***$p<0.0001$ Student's t-test. **B**) Cortical neurons infected with CRISPR-*NPAS4* lentiviruses at DIV1 were immunostained against MAP2 and glutamate decarboxylase 65 (GAD65) at DIV7. Quantification of GAD65 signal was normalized to the number of cells (5 fields per coverslip, 2 coverslips for each genotype in two independent experiments, (N=2). Results (mean ± SEM) are given as percentage of control (Ct). Scale bar: 200µm. **$p=0.0024$. Mann-Whitney test. **C**) Quantification of γ-amino butyric acid (GABA) in culture medium at DIV7of infected control neurons (Ct) and CRISPR-*NPAS4* infected neurons. Results (mean ± SEM) are expressed as percentage of Ct (n=5, N=2). *$p=0.0146$, Student-t test. **D**) Neurons harvested at DIV7 and cell extracts analyzed by Western blotting for GABARα1, GAD65 and GADPH expression. Quantification of GABARα1 and GAD65 were normalized to GAPDH expression. Results (mean ± SEM) are expressed as percentage of Ct (n=8, N=3). *$p=0.049$, $^{\#}p=0.0247$, Student's t-test.

eNeuro Accepted Manuscript

836

837 **Extended Data Figure Legends**

838 **Figure 1-1: Experimental workflow and model characterization**

839 **A**) Experimental design used for the study (E18); neurons were cultured and experiments were
840 mainly carried out after 3 and 7 days in vitro (DIV3 and DIV7). Transcriptome analysis was
841 performed on embryonic cortex (E18) and at DIV3 or DIV7. **B**) APP, APLP1 and APLP2
842 expressions were analyzed by Western blotting at the indicated days of culture in APP+/+
843 neurons. **C**) Quantification of APP, APLP1 and APLP2 protein expression over time in APP+/+
844 neurons. Accumulation is represented as fold change over the signal measured at day 0.
845 Quantification was performed from one neuronal culture **D**) APLP1 and APLP2 expressions are
846 not modified in cortical tissue at E18 and primary neuron cultures at DIV3 and DIV 7 in absence
847 of APP. Expression of APP, APLP1, APLP2 was analyzed by Western blotting of cells lysates
848 from APP+/+ and APP-/- primary neuron cultures. **E**) Samples from primary cultures at DIV7
849 (APP+/+, APP+/- and APP-/- neurons) were probed (Western blotting) with an antibody directed
850 against APP C-terminus for APP C-terminal fragments (CTFs) and AICD. Low and high
851 exposures of a typical blot are shown. Arrows indicate the expected position of APP holoprotein,
852 APP CTFs and AICD.

853 **Figure 1-2: Expression of Egr1 and Egr3 is not modified in APP-/- neurons**

854 Egr1 and Egr3 expressions were evaluated in APP+/+ vs. APP-/- primary neurons at DIV7. **A**)
855 Egr1 mRNA and **B**) Egr3 mRNA levels was measured by qPCR (n=6, N=3) at DIV7. Results
856 (mean ± SEM) are given as percentage of controls (APP+/+) n.s= non-significant, Student's t-
857 test.

858

eNeuro Accepted Manuscript

Figure 2-1: Astrocytes in primary neuron culture and their implication in Npas4 expression.

A) Primary culture of cortical neurons at DIV7. Cultures were immunostained with the neuron specific protein MAP2 (green), the glial specific protein GFAP (red) and the DAPI (light blue). Scale bar = 400µm. **B**) Quantification of neurons (MAP2+) and astrocytes (GFAP+) in the primary cortical culture. At least five fields per coverslip were analyzed for APP+/+ and APP-/- cultures in two independent experiments (n≥5, N=2). Results are expressed as the ratio of MAP2+ (neurons) and GFAP+ (astrocytes) (mean ± s.e.m). n.s= non-significant, Mann-Whitney test. **C**) Western blotting analysis of NPAS4 induction in neurons and astrocytes after depolarization with 50mM potassium chloride (KCl) for 2 hours.

Figure 3-1: Infectivity and toxicity of lentiviral CRISPR-Cas9 vectors

A) Cortical neurons were infected at DIV1 with lentiviruses expressing sgRNAs (Oligo2, Oligo17 or CRISPR-*NPAS4*) or no sgRNA (Ct), SpCas9 and GFP. Cultures were immunostained for MAP2 (red) and DAPI (light blue) at DIV7. Scale bar = 400µm. **B**) Quantification of GFP+ neurons (GFP+/MAP2+) in total neuron population (MAP2+) after lentiviral CRISPR-Cas9 infection with control (Ct), Oligo2, Oligo17 or CRISPR-*NPAS4*. At least five fields were analyzed for each lentiviral vector in two independent experiments (n≥5, N=2). Results are expressed as percentage of GFP+/MAP2+ cells in total MAP2+ cells (mean ± s.e.m). n.s= non-significant, Kruskal-Wallis test and Dunn's multiple comparison test. **C**) Measurement of LDH activity released after infection (DIV7) of primary neuron with control (Ct), Oligo2, Oligo17 or CRISPR-*NPAS4* at DIV7 lentiviral vectors. Background LDH release was determined in non-infected control cultures (NI). Results were expressed as percentage of total LDH release measured in non-infected control cultures (NI) in 2 independent experiments (n=12, N=2).

Figure 5-1: Glutamate responses in APP-/- neurons measured by calcium imaging.

eNeuro Accepted Manuscript

Neuronal activity was measured at DIV7 by calcium imaging. **A**) Left panel. Different calcium responses were observed after stimulation with 50 µM glutamate and classified as described by Prickering and co-workers (Prickering et al. 2008) between neuronal and non-neuronal responses. To note X-axe graduation correspond to 20 sec. Right panel. The proportion of cells displaying Type 1, 2 or 3 response was quantified in three independent experiments (n=9, N=3). n.s.= non-significant. Student-t test. **B**) Normalized fluorescence trace (mean ± SEM) measured in APP+/+ and APP-/- neurons upon perfusion for 150 sec with 50 µM glutamate. The area under curve (AUC) was quantified for 50 neurons per coverslips. A total of 9 coverslips for each genotype was recorded in three independent experiments (N=3). The graph on the right shows AUC expressed as percentage of control (APP+/+). *p=0.0106, Student's t-test.

Figure 5-2: GAD65 positive neurons in primary cortical cultures.

A) Primary culture of cortical neurons after at DIV7. Cultures were immunostained with the neuron specific protein MAP2 (red), GAD65 (dark blue) and DAPI (light blue). Representative 20x micrographs show GAD65 positive neurons (white arrowhead) and GAD65 negative neuron (green arrowhead). **B**) Images (20x objective) were quantified (10 fields per coverslip for each genotype) in three independent cultures (n=30, N=3). Results (mean ± s.e.m) are expressed as percentage of GAD65+ MAP2+ cells (GAD65+ neurons) among all MAP2+ cells (neurons). n.s= non-significant, Mann-Whitney test. Scale bar = 20µm.

Figure 6-1: LTP in hippocampal SC-CA1 pathway in APP-/- mice

Excitatory postsynaptic potentials measured in hippocampal CA1 region of brain slices from APP+/+ (N=9) and APP-/- mice (N=8). **A**) The input-output relationship between fEPSP measured in CA1 stratum radiatum and the intensity of SC stimulation is represented. No significant difference between APP+/+ and APP-/- was observed.

eNeuro Accepted Manuscript

907 **References**

908 Alberini, C.M. (2009). Transcription factors in long-term memory and synaptic plasticity. *Physiol*
909 *Rev* 89(1)**,** 121-145. doi: 10.1152/physrev.00017.2008.

910 Anderson WW, Collingridge GL (2007). Capabilities of the WinLTP data acquisition program
911 extending beyond basic LTP experimental functions. J Neurosci Methods 162:346-356.

912 Aydin, D., Filippov, M.A., Tschape, J.A., Gretz, N., Prinz, M., Eils, R., et al. (2011). Comparative
913 transcriptome profiling of amyloid precursor protein family members in the adult cortex.
914 *BMC Genomics* 12**,** 160. doi: 10.1186/1471-2164-12-160.

915 Belyaev, N.D., Kellett, K.A., Beckett, C., Makova, N.Z., Revett, T.J., Nalivaeva, N.N., et al.
916 (2010). The transcriptionally active amyloid precursor protein (APP) intracellular domain
917 is preferentially produced from the 695 isoform of APP in a {beta}-secretase-dependent
918 pathway. *J Biol Chem* 285(53)**,** 41443-41454. doi: 10.1074/jbc.M110.141390.

919 Ben-Ari, Y. (2002). Excitatory actions of gaba during development: the nature of the nurture. *Nat*
920 *Rev Neurosci* 3(9)**,** 728-739. doi: 10.1038/nrn920.

921 Billnitzer, A.J., Barskaya, I., Yin, C., and Perez, R.G. (2013). APP independent and dependent
922 effects on neurite outgrowth are modulated by the receptor associated protein (RAP). *J*
923 *Neurochem* 124(1)**,** 123-132. doi: 10.1111/jnc.12051.

924 Bloodgood, B.L., Sharma, N., Browne, H.A., Trepman, A.Z., and Greenberg, M.E. (2013). The
925 activity-dependent transcription factor NPAS4 regulates domain-specific inhibition.
926 *Nature* 503(7474)**,** 121-125. doi: 10.1038/nature12743.

927 Born, H.A., Kim, J.Y., Savjani, R.R., Das, P., Dabaghian, Y.A., Guo, Q., et al. (2014). Genetic
928 suppression of transgenic APP rescues Hypersynchronous network activity in a mouse
929 model of Alzeimer's disease. *J Neurosci* 34(11)**,** 3826-3840. doi:
930 10.1523/JNEUROSCI.5171-13.2014.

eNeuro Accepted Manuscript

931 Caceres, J., and Brandan, E. (1997). Interaction between Alzheimer's disease beta A4 precursor
932 protein (APP) and the extracellular matrix: evidence for the participation of heparan
933 sulfate proteoglycans. *J Cell Biochem* 65(2), 145-158.
934 Chen, M., Wang, J., Jiang, J., Zheng, X., Justice, N.J., Wang, K., et al. (2017). APP modulates
935 KCC2 expression and function in hippocampal GABAergic inhibition. *Elife* 6. doi:
936 10.7554/eLife.20142.
937 Cousins, S.L., Hoey, S.E., Anne Stephenson, F., and Perkinton, M.S. (2009). Amyloid precursor
938 protein 695 associates with assembled NR2A- and NR2B-containing NMDA receptors to
939 result in the enhancement of their cell surface delivery. *J Neurochem* 111(6), 1501-1513.
940 doi: 10.1111/j.1471-4159.2009.06424.x.
941 Dawson GR, Seabrook GR, Zheng H, Smith DW, Graham S, O'Dowd G, Bowery BJ, Boyce S,
942 Trumbauer ME, Chen HY, Van Der Ploeg LH, Sirinathsinghji DJ (1999) Age-related
943 cognitive deficits, impaired long-term potentiation and reduction in synaptic marker
944 density in mice lacking the beta-amyloid precursor protein. *Neuroscience* 90:1-13.
945 Deyts, C., Thinakaran, G., and Parent, A.T. (2016). APP Receptor? To Be or Not To Be. *Trends*
946 *Pharmacol Sci* 37(5), 390-411. doi: 10.1016/j.tips.2016.01.005.
947 Doshina, A., Gourgue, F., Onizuka, M., Opsomer, R., Wang, P., Ando, K., et al. (2017). Cortical
948 cells reveal APP as a new player in the regulation of GABAergic neurotransmission. *Sci*
949 *Rep* 7(1), 370. doi: 10.1038/s41598-017-00325-2.
950 Edgar R, Domrachev M, Lash AE (2002) Gene Expression Omnibus: NCBI gene expression and
951 hybridization array data repository. Nucleic Acids Res 30:207-210.
952 Fitzjohn, S.M., Morton, R.A., Kuenzi, F., Davies, C.H., Seabrook, G.R., and Collingridge, G.L.
953 (2000). Similar levels of long-term potentiation in amyloid precursor protein -null and wild-
954 type mice in the CA1 region of picrotoxin treated slices. *Neurosci Lett* 288(1), 9-12.

eNeuro Accepted Manuscript

955 Freude, K.K., Penjwini, M., Davis, J.L., LaFerla, F.M., and Blurton-Jones, M. (2011). Soluble
956 amyloid precursor protein induces rapid neural differentiation of human embryonic stem
957 cells. *J Biol Chem* 286(27)**,** 24264-24274. doi: 10.1074/jbc.M111.227421.
958 Friedman, D., Honig, L.S., and Scarmeas, N. (2012). Seizures and epilepsy in Alzheimer's
959 disease. *CNS Neurosci Ther* 18(4)**,** 285-294. doi: 10.1111/j.1755-5949.2011.00251.x.
960 Grimm, M.O., Mett, J., Stahlmann, C.P., Haupenthal, V.J., Zimmer, V.C., and Hartmann, T.
961 (2013). Neprilysin and Abeta Clearance: Impact of the APP Intracellular Domain in NEP
962 Regulation and Implications in Alzheimer's Disease. *Front Aging Neurosci* 5**,** 98. doi:
963 10.3389/fnagi.2013.00098.
964 Gueli, M.C., and Taibi, G. (2013). Alzheimer's disease: amino acid levels and brain metabolic
965 status. *Neurol Sci* 34(9)**,** 1575-1579. doi: 10.1007/s10072-013-1289-9.
966 Guo, Q., Wang, Z., Li, H., Wiese, M., and Zheng, H. (2012). APP physiological and
967 pathophysiological functions: insights from animal models. *Cell Res* 22(1)**,** 78-89. doi:
968 10.1038/cr.2011.116.
969 Heckl, D., Kowalczyk, M.S., Yudovich, D., Belizaire, R., Puram, R.V., McConkey, M.E., et al.
970 (2014). Generation of mouse models of myeloid malignancy with combinatorial genetic
971 lesions using CRISPR-Cas9 genome editing. *Nat Biotechnol* 32(9)**,** 941-946. doi:
972 10.1038/nbt.2951.
973 Hendrickx A, Pierrot N, Tasiaux B, Schakman O, Brion JP, Kienlen-Campard P, De SC, Octave
974 JN (2013) Epigenetic Induction of EGR-1 Expression by the Amyloid Precursor Protein
975 during Exposure to Novelty. PLoS One 8:e74305.
976 Hendrickx A, Pierrot N, Tasiaux B, Schakman O, Kienlen-Campard P, De SC, Octave JN (2014)
977 Epigenetic regulations of immediate early genes expression involved in memory
978 formation by the amyloid precursor protein of Alzheimer disease. PLoS One 9:e99467.

eNeuro Accepted Manuscript

Hicks, D.A., Makova, N.Z., Gough, M., Parkin, E.T., Nalivaeva, N.N., and Turner, A.J. (2013). The amyloid precursor protein represses expression of acetylcholinesterase in neuronal cell lines. *J Biol Chem* 288(36), 26039-26051. doi: 10.1074/jbc.M113.461269.

Hoe, H.S., Fu, Z., Makarova, A., Lee, J.Y., Lu, C., Feng, L., et al. (2009a). The effects of amyloid precursor protein on postsynaptic composition and activity. *J Biol Chem* 284(13), 8495-8506. doi: 10.1074/jbc.M900141200.

Hoe, H.S., Lee, K.J., Carney, R.S., Lee, J., Markova, A., Lee, J.Y., et al. (2009b). Interaction of reelin with amyloid precursor protein promotes neurite outgrowth. *J Neurosci* 29(23), 7459-7473. doi: 10.1523/JNEUROSCI.4872-08.2009.

Hsieh, H., Boehm, J., Sato, C., Iwatsubo, T., Tomita, T., Sisodia, S., et al. (2006). AMPAR removal underlies Abeta-induced synaptic depression and dendritic spine loss. *Neuron* 52(5), 831-843. doi: 10.1016/j.neuron.2006.10.035.

Hu, Y., Hung, A.C., Cui, H., Dawkins, E., Bolos, M., Foa, L., et al. (2013). Role of cystatin C in amyloid precursor protein-induced proliferation of neural stem/progenitor cells. *J Biol Chem* 288(26), 18853-18862. doi: 10.1074/jbc.M112.443671.

Huysseune, S., Kienlen-Campard, P., and Octave, J.N. (2007). Fe65 does not stabilize AICD during activation of transcription in a luciferase assay. *Biochem Biophys Res Commun* 361(2), 317-322. doi: 10.1016/j.bbrc.2007.06.186.

Jedlicka P, Owen M, Vnencak M, Tschape JA, Hick M, Muller UC, Deller T (2012) Functional consequences of the lack of amyloid precursor protein in the mouse dentate gyrus in vivo. *Exp Brain Res* 217:441-447.

Jinek, M., Chylinski, K., Fonfara, I., Hauer, M., Doudna, J.A., and Charpentier, E. (2012). A programmable dual-RNA-guided DNA endonuclease in adaptive bacterial immunity. *Science* 337(6096), 816-821. doi: 10.1126/science.1225829.

Kamenetz, F., Tomita, T., Hsieh, H., Seabrook, G., Borchelt, D., Iwatsubo, T., et al. (2003). APP processing and synaptic function. *Neuron* 37(6), 925-937.

eNeuro Accepted Manuscript

1005 Kanehisa, M., and Goto, S. (2000). KEGG: kyoto encyclopedia of genes and genomes. *Nucleic*
1006 *Acids Res* 28(1), 27-30.
1007 Kimberly, W.T., Zheng, J.B., Town, T., Flavell, R.A., and Selkoe, D.J. (2005). Physiological
1008 regulation of the beta-amyloid precursor protein signaling domain by c-Jun N-terminal
1009 kinase JNK3 during neuronal differentiation. *J Neurosci* 25(23), 5533-5543. doi:
1010 10.1523/JNEUROSCI.4883-04.2005.
1011 Klevanski, M., Herrmann, U., Weyer, S.W., Fol, R., Cartier, N., Wolfer, D.P., et al. (2015). The
1012 APP Intracellular Domain Is Required for Normal Synaptic Morphology, Synaptic
1013 Plasticity, and Hippocampus-Dependent Behavior. *J Neurosci* 35(49), 16018-16033. doi:
1014 10.1523/JNEUROSCI.2009-15.2015.
1015 Larson J, Munkacsy E (2015) Theta-burst LTP. Brain Res 1621:38-50.
1016 Lee, K.J., Moussa, C.E., Lee, Y., Sung, Y., Howell, B.W., Turner, R.S., et al. (2010). Beta
1017 amyloid-independent role of amyloid precursor protein in generation and maintenance of
1018 dendritic spines. *Neuroscience* 169(1), 344-356. doi:
1019 10.1016/j.neuroscience.2010.04.078.
1020 Lepannetier S, Gualdani R, Tempesta S, Schakman O, Seghers F, Kreis A, Yerna X, Slimi A, de
1021 CM, Tajeddine N, Voets T, Bon RS, Beech DJ, Tissir F, Gailly P (2018) Activation of
1022 TRPC1 Channel by Metabotropic Glutamate Receptor mGluR5 Modulates Synaptic
1023 Plasticity and Spatial Working Memory. Front Cell Neurosci 12:318.
1024 Leslie, J.H., and Nedivi, E. (2011). Activity-regulated genes as mediators of neural circuit
1025 plasticity. *Prog Neurobiol* 94(3), 223-237. doi: 10.1016/j.pneurobio.2011.05.002.
1026 Lin, Y., Bloodgood, B.L., Hauser, J.L., Lapan, A.D., Koon, A.C., Kim, T.K., et al. (2008). Activity-
1027 dependent regulation of inhibitory synapse development by Npas4. *Nature* 455(7217),
1028 1198-1204. doi: 10.1038/nature07319.
1029 Loebrich, S., and Nedivi, E. (2009). The function of activity-regulated genes in the nervous
1030 system. *Physiol Rev* 89(4), 1079-1103. doi: 10.1152/physrev.00013.2009.

eNeuro Accepted Manuscript

1031 Milosch, N., Tanriover, G., Kundu, A., Rami, A., Francois, J.C., Baumkotter, F., et al. (2014).
1032 Holo-APP and G-protein-mediated signaling are required for sAPPalpha-induced
1033 activation of the Akt survival pathway. *Cell Death Dis* 5**,** e1391. doi:
1034 10.1038/cddis.2014.352.
1035 Miyashita, A., Hatsuta, H., Kikuchi, M., Nakaya, A., Saito, Y., Tsukie, T., et al. (2014). Genes
1036 associated with the progression of neurofibrillary tangles in Alzheimer's disease. *Transl*
1037 *Psychiatry* 4**,** e396. doi: 10.1038/tp.2014.35.
1038 Mizukami K, Ikonomovic MD, Grayson DR, Sheffield R, Armstrong DM (1998)
1039 Immunohistochemical study of GABAA receptor alpha1 subunit in the hippocampal
1040 formation of aged brains with Alzheimer-related neuropathologic changes. Brain Res
1041 799:148-155.
1042 Muller, U., Cristina, N., Li, Z.W., Wolfer, D.P., Lipp, H.P., Rulicke, T., et al. (1994). Behavioral
1043 and anatomical deficits in mice homozygous for a modified beta-amyloid precursor
1044 protein gene. *Cell* 79(5)**,** 755-765.
1045 Muller, U.C., Deller, T., and Korte, M. (2017). Not just amyloid: physiological functions of the
1046 amyloid precursor protein family. *Nat Rev Neurosci* 18(5)**,** 281-298. doi:
1047 10.1038/nrn.2017.29.
1048 Muller, U.C., Pietrzik, C.U., and Deller, T. (2012). The physiological functions of the beta-amyloid
1049 precursor protein APP. *Exp Brain Res* 217(3-4)**,** 325-329. doi: 10.1007/s00221-012-
1050 3039-2.
1051 Muller, U.C., and Zheng, H. (2012). Physiological functions of APP family proteins. *Cold Spring*
1052 *Harb Perspect Med* 2(2)**,** a006288. doi: 10.1101/cshperspect.a006288.
1053 Pardossi-Piquard, R., and Checler, F. (2012). The physiology of the beta-amyloid precursor
1054 protein intracellular domain AICD. *J Neurochem* 120 Suppl 1**,** 109-124. doi:
1055 10.1111/j.1471-4159.2011.07475.x.

eNeuro Accepted Manuscript

1056 Pickering, M., Pickering, B.W., Murphy, K.J., and O'Connor, J.J. (2008). Discrimination of cell
1057 types in mixed cortical culture using calcium imaging: a comparison to
1058 immunocytochemical labeling. *J Neurosci Methods* 173(1), 27-33. doi:
1059 10.1016/j.jneumeth.2008.05.014.
1060 Pierrot, N., Tyteca, D., D'Auria, L., Dewachter, I., Gailly, P., Hendrickx, A., et al. (2013). Amyloid
1061 precursor protein controls cholesterol turnover needed for neuronal activity. *EMBO Mol*
1062 *Med* 5(4), 608-625. doi: 10.1002/emmm.201202215.
1063 Priller, C., Bauer, T., Mitteregger, G., Krebs, B., Kretzschmar, H.A., and Herms, J. (2006).
1064 Synapse formation and function is modulated by the amyloid precursor protein. *J*
1065 *Neurosci* 26(27), 7212-7221. doi: 10.1523/JNEUROSCI.1450-06.2006.
1066 Puzzo, D., Privitera, L., Fa, M., Staniszewski, A., Hashimoto, G., Aziz, F., et al. (2011).
1067 Endogenous amyloid-beta is necessary for hippocampal synaptic plasticity and memory.
1068 *Ann Neurol* 69(5), 819-830. doi: 10.1002/ana.22313.
1069 Rice HC, de MD, Schreurs A, Frere S, Van M, I, Volkov AN, Creemers E, Vertkin I, Nys J,
1070 Ranaivoson FM, Comoletti D, Savas JN, Remaut H, Balschun D, Wierda KD, Slutsky I,
1071 Farrow K, De SB, de WJ (2019) Secreted amyloid-beta precursor protein functions as a
1072 GABABR1a ligand to modulate synaptic transmission. Science 363.
1073 Ring, S., Weyer, S.W., Kilian, S.B., Waldron, E., Pietrzik, C.U., Filippov, M.A., et al. (2007). The
1074 secreted beta-amyloid precursor protein ectodomain APPs alpha is sufficient to rescue
1075 the anatomical, behavioral, and electrophysiological abnormalities of APP-deficient mice.
1076 *J Neurosci* 27(29), 7817-7826. doi: 10.1523/JNEUROSCI.1026-07.2007.
1077 Ritchie, M.E., Phipson, B., Wu, D., Hu, Y., Law, C.W., Shi, W., et al. (2015). limma powers
1078 differential expression analyses for RNA-sequencing and microarray studies. *Nucleic*
1079 *Acids Res* 43(7), e47. doi: 10.1093/nar/gkv007.

eNeuro Accepted Manuscript

1080 Santos, S.F., Pierrot, N., Morel, N., Gailly, P., Sindic, C., and Octave, J.N. (2009). Expression of
1081 human amyloid precursor protein in rat cortical neurons inhibits calcium oscillations. *J*
1082 *Neurosci* 29(15), 4708-4718. doi: 10.1523/JNEUROSCI.4917-08.2009.
1083 Seabrook, G.R., Smith, D.W., Bowery, B.J., Easter, A., Reynolds, T., Fitzjohn, S.M., et al.
1084 (1999). Mechanisms contributing to the deficits in hippocampal synaptic plasticity in mice
1085 lacking amyloid precursor protein. *Neuropharmacology* 38(3), 349-359.
1086 Senechal, Y., Kelly, P.H., Cryan, J.F., Natt, F., and Dev, K.K. (2007). Amyloid precursor protein
1087 knockdown by siRNA impairs spontaneous alternation in adult mice. *J Neurochem*
1088 102(6), 1928-1940. doi: 10.1111/j.1471-4159.2007.04672.x.
1089 Shariati, S.A., and De Strooper, B. (2013). Redundancy and divergence in the amyloid precursor
1090 protein family. *FEBS Lett* 587(13), 2036-2045. doi: 10.1016/j.febslet.2013.05.026.
1091 Sim, S., Antolin, S., Lin, C.W., Lin, Y., and Lois, C. (2013). Increased cell-intrinsic excitability
1092 induces synaptic changes in new neurons in the adult dentate gyrus that require Npas4.
1093 *J Neurosci* 33(18), 7928-7940. doi: 10.1523/JNEUROSCI.1571-12.2013.
1094 Snyder, E.M., Nong, Y., Almeida, C.G., Paul, S., Moran, T., Choi, E.Y., et al. (2005). Regulation
1095 of NMDA receptor trafficking by amyloid-beta. *Nat Neurosci* 8(8), 1051-1058. doi:
1096 10.1038/nn1503.
1097 Spiegel, I., Mardinly, A.R., Gabel, H.W., Bazinet, J.E., Couch, C.H., Tzeng, C.P., et al. (2014).
1098 Npas4 regulates excitatory-inhibitory balance within neural circuits through cell-type-
1099 specific gene programs. *Cell* 157(5), 1216-1229. doi: 10.1016/j.cell.2014.03.058.
1100 Stanga, S., Zanou, N., Audouard, E., Tasiaux, B., Contino, S., Vandermeulen, G., et al. (2016).
1101 APP-dependent glial cell line-derived neurotrophic factor gene expression drives
1102 neuromuscular junction formation. *FASEB J* 30(5), 1696-1711. doi: 10.1096/fj.15-
1103 278739.
1104 Sun, X., and Lin, Y. (2016). Npas4: Linking Neuronal Activity to Memory. *Trends Neurosci* 39(4),
1105 264-275. doi: 10.1016/j.tins.2016.02.003.

eNeuro Accepted Manuscript

1106 Taylor CJ, Ireland DR, Ballagh I, Bourne K, Marechal NM, Turner PR, Bilkey DK, Tate WP,
1107 Abraham WC (2008) Endogenous secreted amyloid precursor protein-alpha regulates
1108 hippocampal NMDA receptor function, long-term potentiation and spatial memory.
1109 Neurobiol Dis 31:250-260.
1110 Tyan, S.H., Shih, A.Y., Walsh, J.J., Maruyama, H., Sarsoza, F., Ku, L., et al. (2012). Amyloid
1111 precursor protein (APP) regulates synaptic structure and function. *Mol Cell Neurosci*
1112 51(1-2), 43-52. doi: 10.1016/j.mcn.2012.07.009.
1113 Vela J, Gutierrez A, Vitorica J, Ruano D (2003) Rat hippocampal GABAergic molecular markers
1114 are differentially affected by ageing. J Neurochem 85:368-377.
1115 Wang B, Wang Z, Sun L, Yang L, Li H, Cole AL, Rodriguez-Rivera J, Lu HC, Zheng H (2014)
1116 The amyloid precursor protein controls adult hippocampal neurogenesis through
1117 GABAergic interneurons. *J Neurosci* 34:13314-13325.
1118 Wang Z, Jackson RJ, Hong W, Taylor WM, Corbett GT, Moreno A, Liu W, Li S, Frosch MP,
1119 Slutsky I, Young-Pearse TL, Spires-Jones TL, Walsh DM (2017) Human Brain-Derived
1120 Abeta Oligomers Bind to Synapses and Disrupt Synaptic Activity in a Manner That
1121 Requires APP. *J Neurosci* 37:11947-11966.
1122 West, A.E., and Greenberg, M.E. (2011). Neuronal activity-regulated gene transcription in
1123 synapse development and cognitive function. *Cold Spring Harb Perspect Biol* 3(6). doi:
1124 10.1101/cshperspect.a005744.
1125 Weyer, S.W., Zagrebelsky, M., Herrmann, U., Hick, M., Ganss, L., Gobbert, J., et al. (2014).
1126 Comparative analysis of single and combined APP/APLP knockouts reveals reduced
1127 spine density in APP-KO mice that is prevented by APPsalpha expression. *Acta*
1128 *Neuropathol Commun* 2, 36. doi: 10.1186/2051-5960-2-36.
1129 White, A.R., Zheng, H., Galatis, D., Maher, F., Hesse, L., Multhaup, G., et al. (1998). Survival of
1130 cultured neurons from amyloid precursor protein knock-out mice against Alzheimer's
1131 amyloid-beta toxicity and oxidative stress. *J Neurosci* 18(16), 6207-6217.

eNeuro Accepted Manuscript

1132 Wu, D., Lim, E., Vaillant, F., Asselin-Labat, M.L., Visvader, J.E., and Smyth, G.K. (2010).
1133 ROAST: rotation gene set tests for complex microarray experiments. *Bioinformatics*
1134 26(17), 2176-2182. doi: 10.1093/bioinformatics/btq401.
1135 Yoshiike Y, Kimura T, Yamashita S, Furudate H, Mizoroki T, Murayama M, Takashima A (2008)
1136 GABA(A) receptor-mediated acceleration of aging-associated memory decline in
1137 APP/PS1 mice and its pharmacological treatment by picrotoxin. PLoS One 3:e3029.
1138 Young-Pearse, T.L., Bai, J., Chang, R., Zheng, J.B., LoTurco, J.J., and Selkoe, D.J. (2007). A
1139 critical function for beta-amyloid precursor protein in neuronal migration revealed by in
1140 utero RNA interference. *J Neurosci* 27(52), 14459-14469. doi:
1141 10.1523/JNEUROSCI.4701-07.2007.
1142 Zheng, H., Jiang, M., Trumbauer, M.E., Sirinathsinghji, D.J., Hopkins, R., Smith, D.W., et al.
1143 (1995). beta-Amyloid precursor protein-deficient mice show reactive gliosis and
1144 decreased locomotor activity. *Cell* 81(4), 525-531.
1145 Zou, C., Crux, S., Marinesco, S., Montagna, E., Sgobio, C., Shi, Y., et al. (2016). Amyloid
1146 precursor protein maintains constitutive and adaptive plasticity of dendritic spines in adult
1147 brain by regulating D-serine homeostasis. *EMBO J* 35(20), 2213-2222. doi:
1148 10.15252/embj.201694085.

1149

eNeuro Accepted Manuscript

Figure 1

A

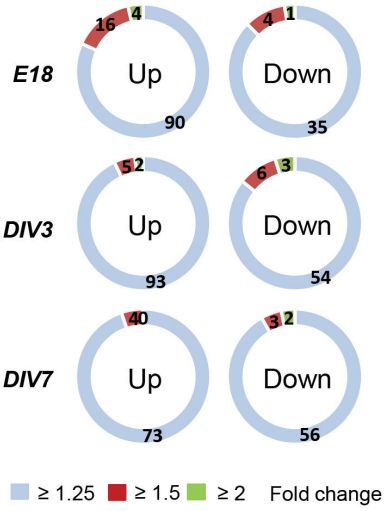

B

KEGG Pathways

E18	Nb. Genes	Direction	p-value	FDR	Mixed p-value
Base excision repair	32	Up	0.008	0.9845	0.465
p53 signaling pathway	70	Up	0.033	0.9845	0.545
Terpenoid backbone biosynthesis	14	*Down*	0.109	0.9845	0.297
Small cell lung cancer	88	Up	0.109	0.9845	0.496
Pyrimidine metabolism	96	Up	0.121	0.9845	0.632
DIV3					
Proteasome	42	Up	0.034	0.9953	0.784
RIG-I-like receptor signaling pathway	67	*Down*	0.042	0.9953	0.821
Terpenoid backbone biosynthesis	14	Up	0.06	0.9953	0.397
Glycosaminoglycan biosynthesis	14	Up	0.067	0.9953	0.557
Steroid biosynthesis	17	Up	0.094	0.9953	0.013
DIV7					
Homologous recombination	26	*Down*	0.226	0.9995	0.746
Glycosylphosphatidylinositol (GPI)-anchor biosynthesis	23	*Down*	0.279	0.9995	0.576
Glycosaminoglycan biosynthesis - keratan sulfate	14	Up	0.304	0.9995	0.543
ECM-receptor interaction	83	*Down*	0.307	0.9995	0.471
Long-term potentiation	64	Up	0.317	0.9995	0.76

C

DIV7	Gene symbol	Fold change *
Immediate Early Genes (IEGs)	*App*	0,05
	Ier2	0,52
	Arc	0,56
	Npas4	**0,57**
	Fosb	0,57
	Fos	0,60
	Egr1	0,66
	Egr2	0,74
	Egr3	0,77
	Egr4	0,78

** linear fold change (APP-/- vs. APP+/+)*

D

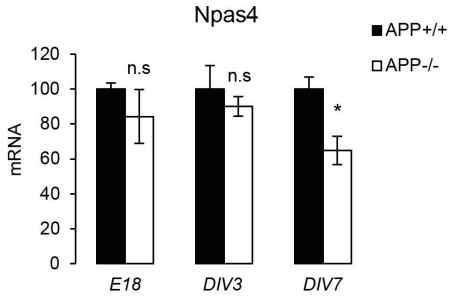

eNeuro Accepted Manuscript

Figure 2

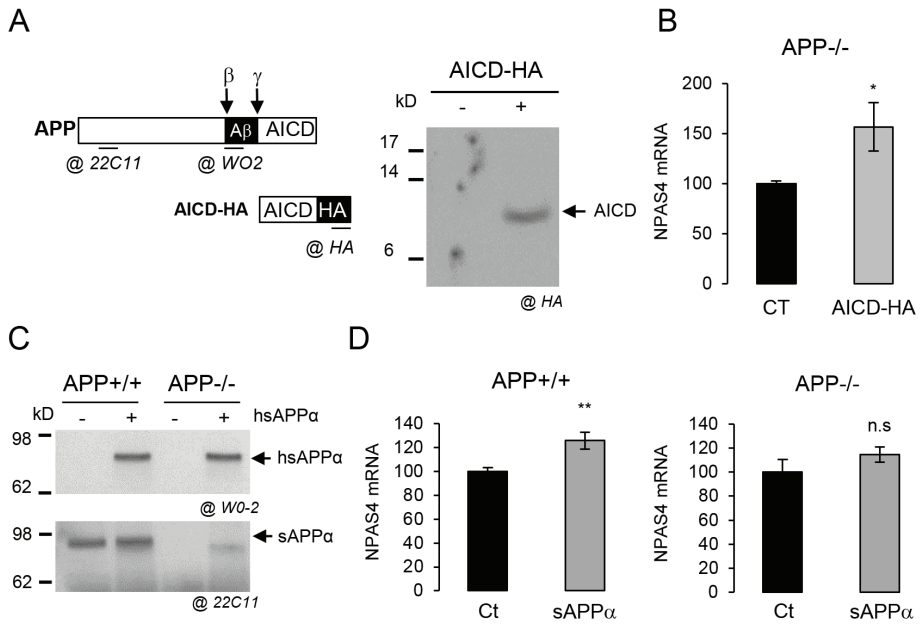

eNeuro Accepted Manuscript

Figure 3

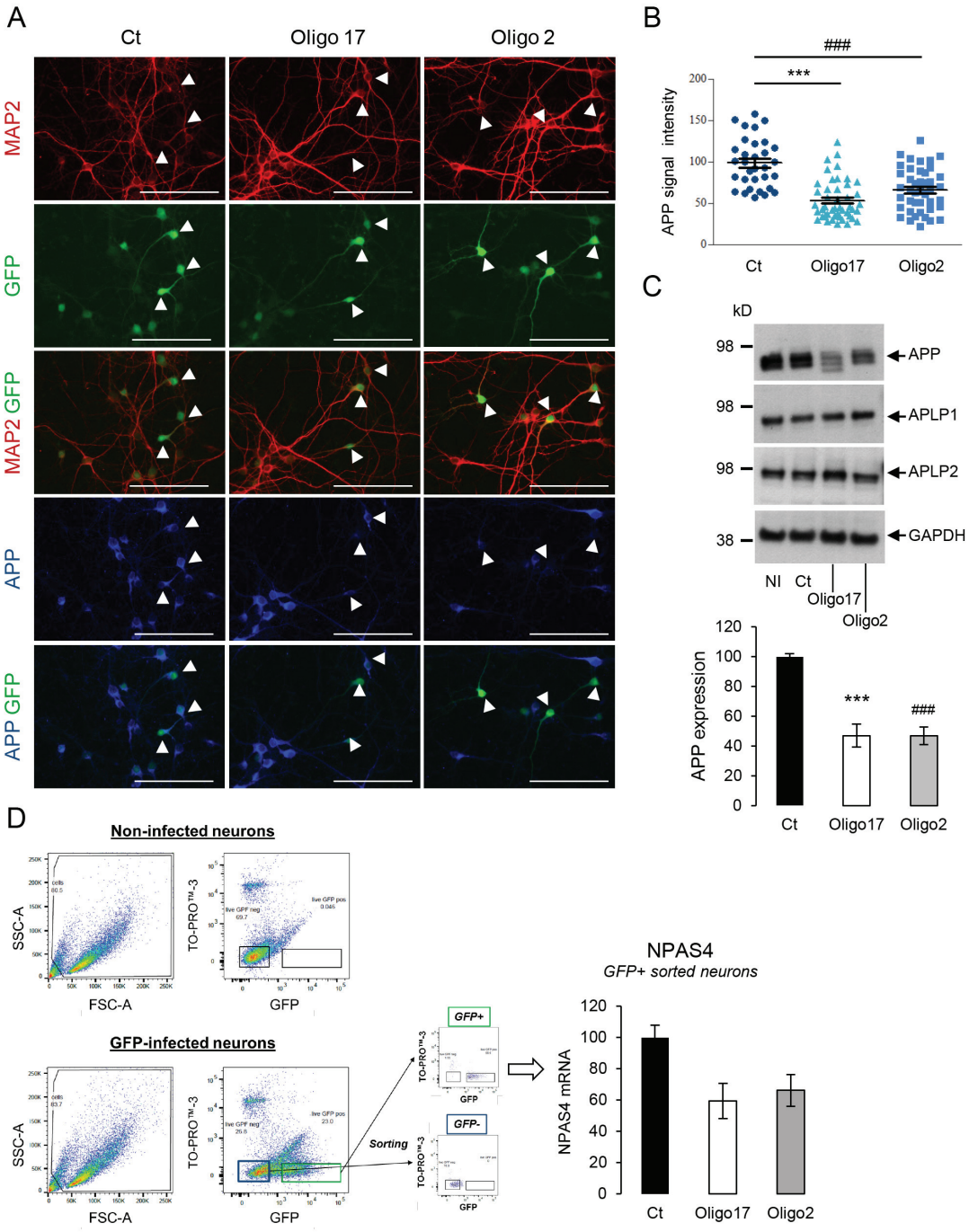

eNeuro Accepted Manuscript

Figure 4

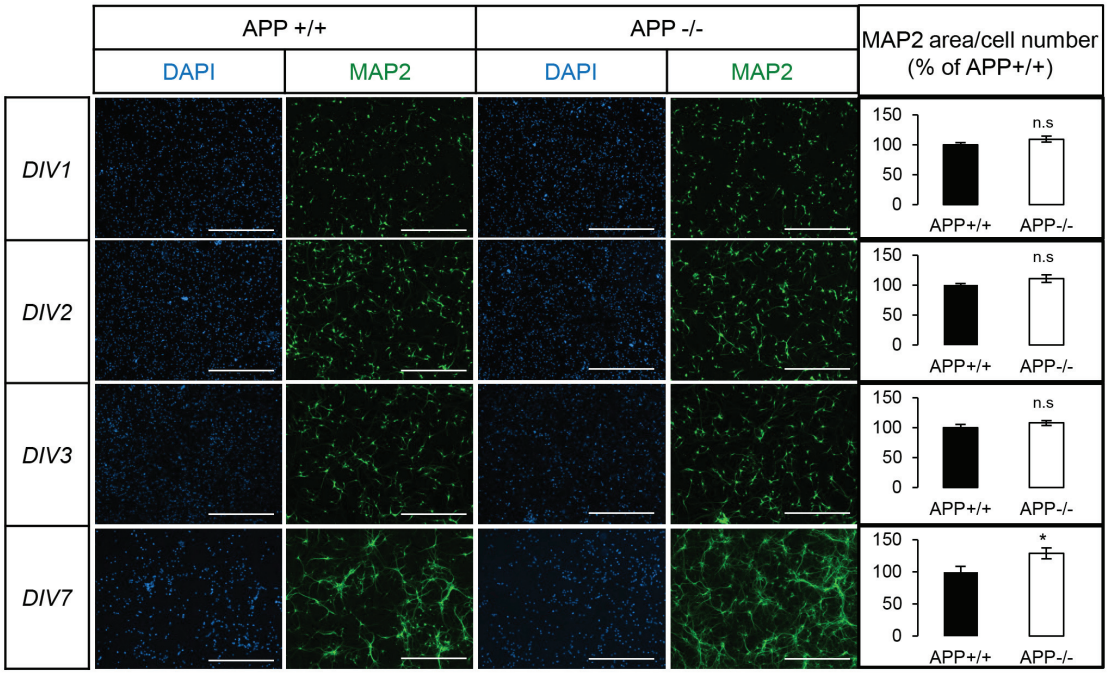

eNeuro Accepted Manuscript

Figure 5

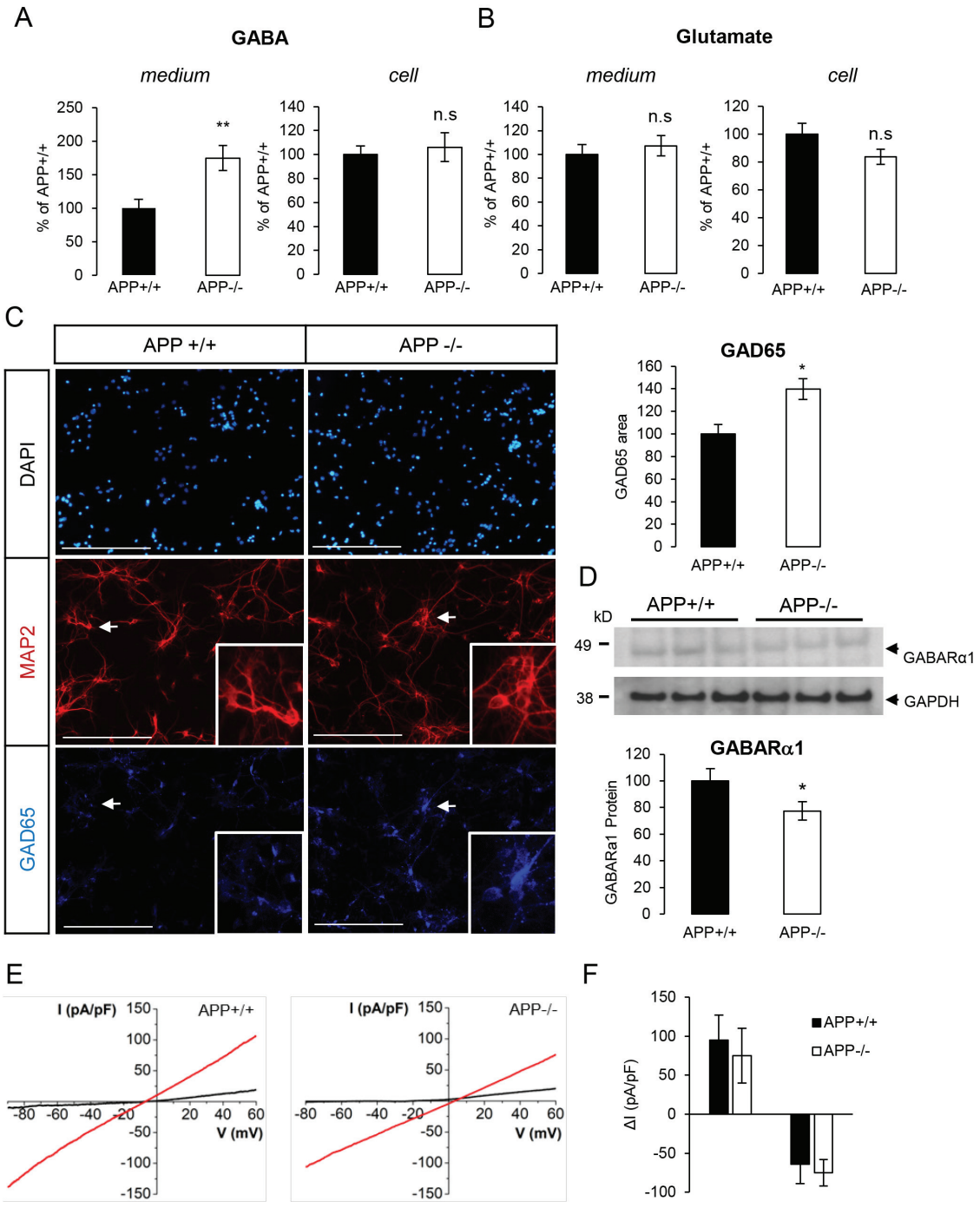

eNeuro Accepted Manuscript

Figure 6

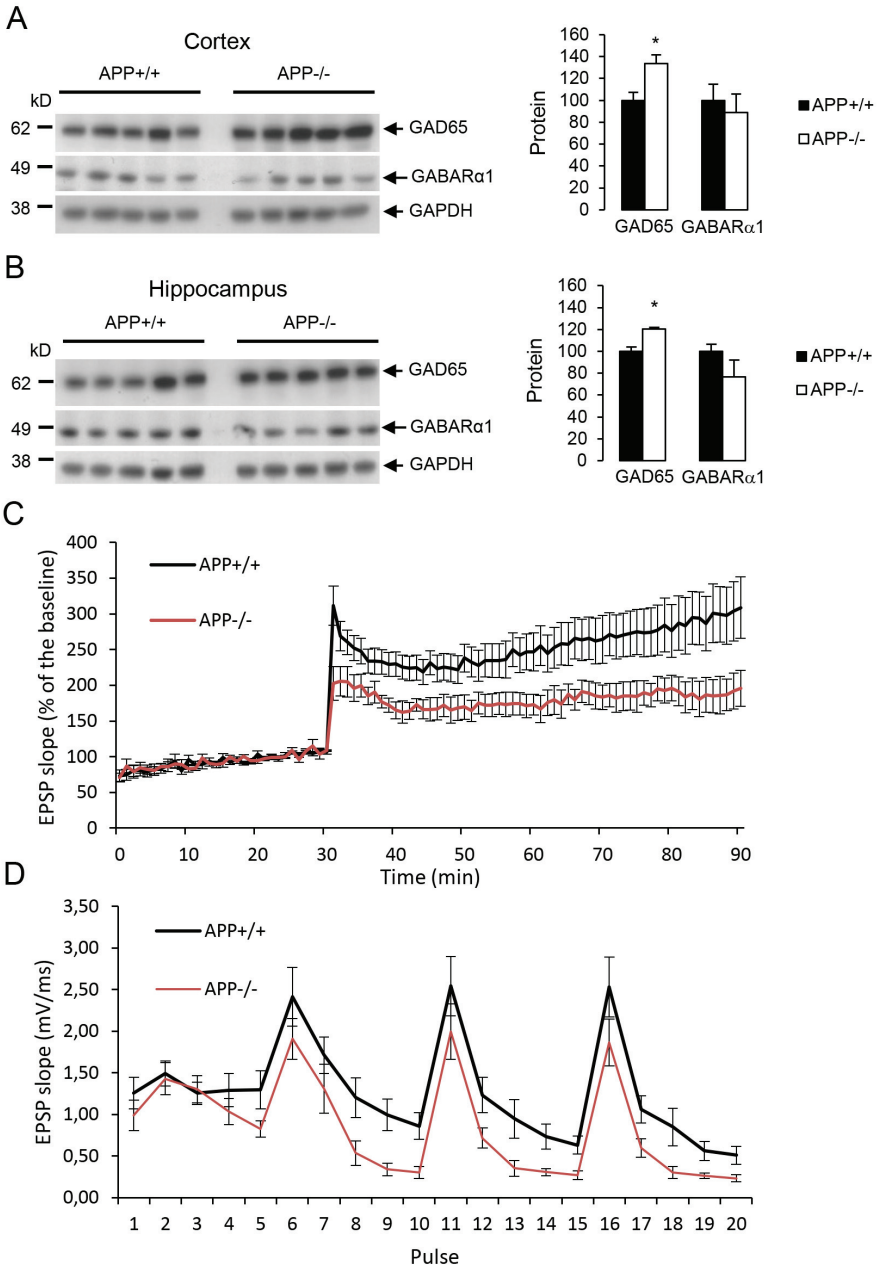

eNeuro Accepted Manuscript
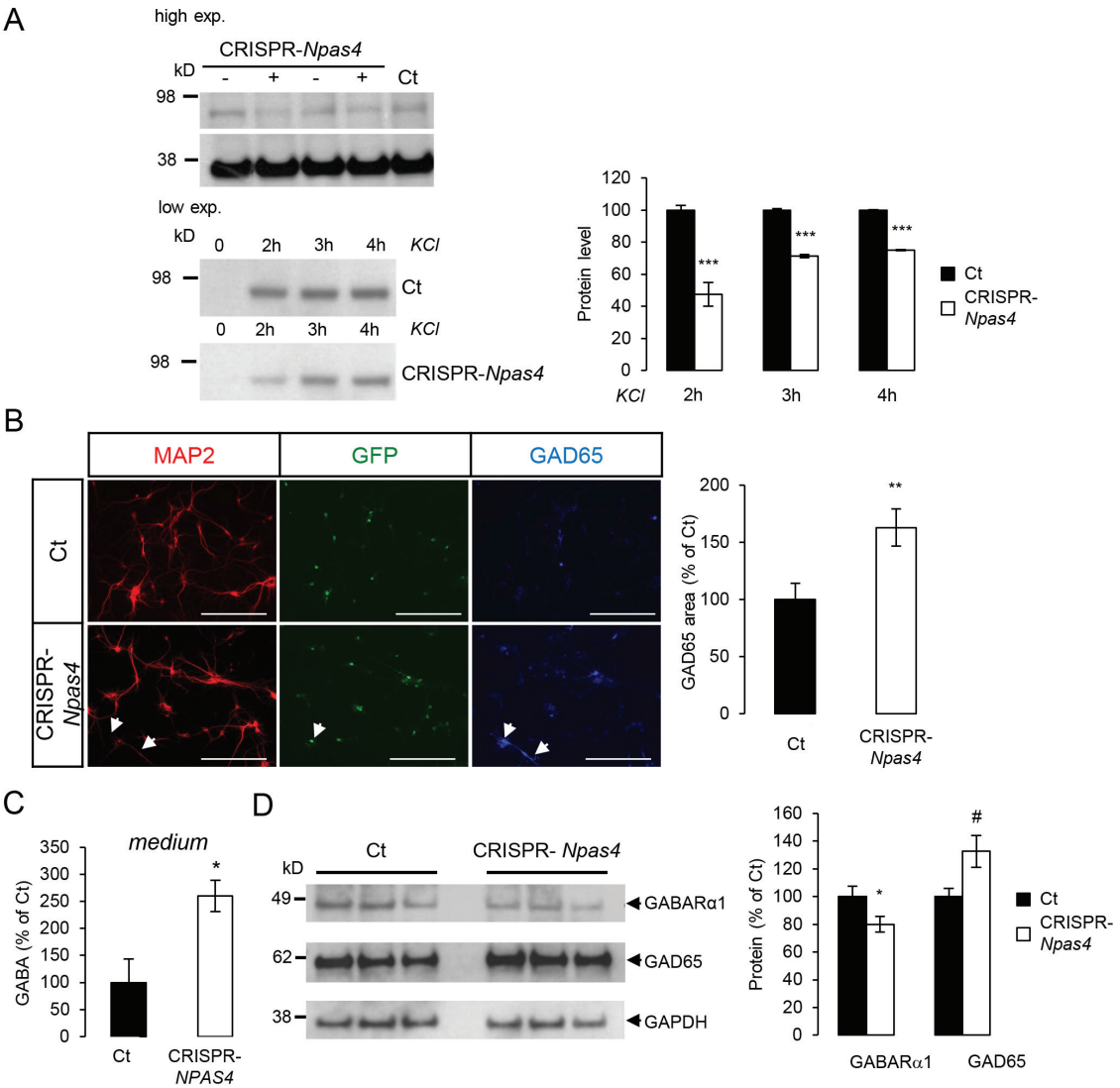
Figure 7